2015

Comparison of 3D and 4D CBCT for the Localization of Moving Targets

Runyon Colie Woods
Louisiana State University and Agricultural and Mechanical College

COMPARISON OF 3D AND 4D CBCT FOR THE LOCALIZATION OF MOVING TARGETS

A Thesis

Submitted to the Graduate Faculty of the
Louisiana State University and
Agricultural and Mechanical College
in partial fulfillment of the
requirements for the degree of
Master of Science

in

The Department of Physics and Astronomy

by
Runyon Colie Woods
B.S., University of North Carolina Wilmington, 2012
August 2015

ACKNOWLEDGMENT

First I must say thank you to all of the LSU and Mary Bird Perkins medical physics faculty, staff and students for the past 3 years in graduate school earing my degree. In particular, my advisor Dr. Fontenot has been a constant source of expertise and supportive input throughout my time performing research under him. Also, my committee members consisting of Dr. Matthews, Dr. Zhang, and Mr. Chu for their help and insight in my work. Last, but certainly not least, I cannot say thank you enough to the therapist Tiffany Shelton for performing all of the manual registrations and help with XVI. Without all of you, this project would have not succeeded.

I send my love to my family for trusting and aiding me throughout the last 3 years in graduate school. My mother for her love, concern, care, and unconditional support: I will love you forever, like you for always, and as long as I'm living, your baby I'll be. My father for his love, steadfast advice, moral guidance, and resolve: I will always love you and by the bye, when I feel the wind on my face, I will stop and think of you. Lastly, my brother Nicholas for his invaluable input and encouragement, but more than anything, the fact that he is the best example of what I should strive to become. You have always been a role model to me and you continue to be such.

Finally, I must say that the woman that I love, Kelly Donoghue, has made these last 3 years alone in Louisiana as happy as they could have been. You are a strong, beautiful, and intelligent woman that I am proud of on a daily basis. I hope that I can one day make you as proud as you make me. I cannot wait for our future together in Chapel Hill. Last but not least, I can't forget my puppy Molly. Thank you for always greeting me with a lick to the face no matter how late I got home.

TABLE OF CONTENTS

LIST OF TABLES

LIST OF FIGURES

ABSTRACT

Purpose: Compare the localization accuracy of 3D cone beam computed tomography (CBCT) and 4D CBCT for a dynamic respiratory phantom, considering cases with and without respiratory variations between planning and treatment.

Methods and Materials: A respiratory phantom was imaged using 3D CBCT and 4D CBCT. Measurements of the amplitude of motion in 3D CBCT and 4D CBCT and size of the sphere at its exhale position in 4D CBCT were acquired. The phantom was then misaligned by known distances relative to a reference position. 3D CBCT and 4D CBCT were used to re-align the phantom by comparing localization images to reference images. Because the ideal 4D CBCT registration approach was to be determined, multiple localization-reference pairs of images were examined. Comparison was performed for multiple respiratory waveforms at two amplitudes as well as for waveforms where amplitudes were increased or decreased by 30%, simulating changes in respiratory behavior between simulation and localization. Error of localization trials was defined as the difference between the recommended table shifts and the known displacement.

Results: Measurements of the respiratory amplitude were underestimated for all cases. Measurement of the sphere diameter exhibited < 2 mm error. Localization errors were less than 2.6 mm for all cases. When the motion amplitude was the same during localization as planning, automatic registration of the exhale frame from the 4D CBCT to the reference exhale frame had the smallest error in localization of 0.54 ± 0.03 mm. However, automatic registration of the 4D CBCT AIP to the reference AIP had the smallest errors when the motion amplitude changed between planning and localization, 1.59 ± 0.12 mm for the +30% amplitude change and 0.69 ± 0.02 mm for the -30% amplitude change.

Conclusion: Because lung tumor motion amplitude throughout treatment may vary between planning and treatment, the use of 4D CBCT AIP registered to reference AIP was recommended for localization. 4D CBCT provided additional benefits compared to 3D CBCT of substantial reduction in target blurring and verification of respiratory motion characteristics prior to treatment.

CHAPTER 1: BACKGROUND AND INTRODUCTION

1.1 STEREOTACTIC BODY RADIATION THERAPY

Stereotactic body radiation therapy (SBRT) is a specialized treatment in radiation therapy that implements a smaller number of fractions of larger dose in a relatively short amount of time. This hypofractionation is used because it has shown to have a more potent biological effect in tumor cells (Timmerman 2008). In order to achieve such a biological effective dose (BED), larger doses are given in much fewer fractions compared to conventional radiation therapy. Where a conventional IMRT treatment can range anywhere from 1.8 to 3 Gy/frac over 10 to 30 fractions, a SBRT plan will use anywhere from 6 to 12 Gy/fraction over 1 to 5 fractions (Benedict 2010). By changing the way radiation is delivered, SBRT can provide a clinical advantage over conventional treatment by reducing dose to normal tissue and critical structures, while keeping a high dose to the tumor.

A plan for SBRT typically uses multiple overlapping beams or arcs centered on the tumor to deliver a large dose to the tumor with sharp dose fall of off, reducing the radiation delivered to the healthy tissue around the tumor. The irradiation margins around the tumor are on the order of millimeters for SBRT compared to centimeters for conventional radiation therapy (Benedict 2010). Margin guidelines follow ICRU Report 50 for a gross tumor volume (GTV) contour around the visible tumor; a clinical target volume (CTV) is expanded from the GTV to account for microscopic involvement, although this step is sometimes avoided in SBRT. Two more margins are added, one for the expansion of the CTV to account for target motion, called the internal target volume (ITV), and the other for the expansion of the ITV to the planning target volume (PTV) to account for positional set up errors (ICRU 1993). The isodose lines tightly

converge around a tumor in the lung SBRT plan in Figure 1.1, demonstrating the sharp dose fall off from the multiple beams used for delivery.

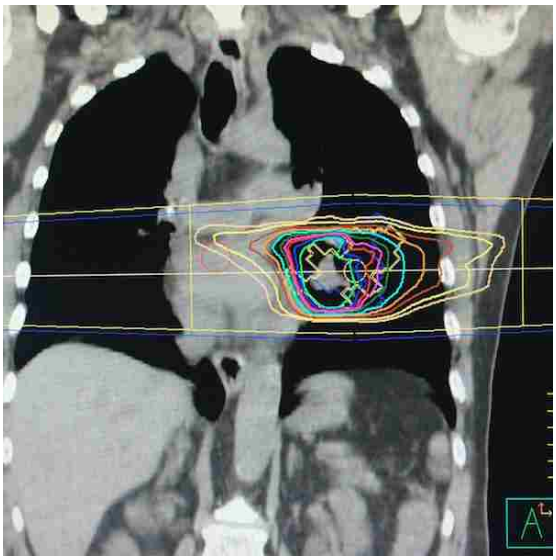

Figure 1.1: Isodose lines around a lung tumor showcasing a steep dose gradient typical in SBRT.

SBRT is used to treat tumors in the liver, on the spine, and in the lung (Benedict 2010). For lung treatments, SBRT is effective for treatments of early stage, inoperable non-small cell lung cancer (NSCLC) (Wulf 2000, Nagata 2002, Murray 2007, Timmerman 2007). Lung tumors are subject to regular respiratory motion that must be taken into account during planning and treatment. Tumors may move more than 4 cm during a breathing cycle, but typically the average motion is 1 cm to 2 cm depending on their location in the lung (Liu 2007, Poulsen 2008).

SBRT requires accuracy throughout the treatment process. This is accomplished through the use of rigorous immobilization, high resolution imaging for treatment planning, and in-room image guidance. Respiratory motion introduces error despite these methods, although some have been improved to further reduce uncertainty (Keall 2006). Most important of these is the accurate alignment of the patient's tumor with the radiation beam through the use of imaging

systems in the treatment vault (Benedict 2010). This process is called image guidance (or image guided radiation therapy). Image guidance must be very reliable when used for SBRT because even a slight misalignment of target and field could greatly under-dose the tumor and overdose healthy tissue.

1.2 IMAGE GUIDED RADIATION THERAPY

In short, image guided radiation therapy (IGRT) is a broad description for the use of imaging during a course of radiation therapy to verify alignment of a beam of radiation to the imaging coordinates from the treatment planning process. IGRT has 3 major components that are necessary for implementation: a reference image, a localization image, and an image registration method.

The purpose of the reference image is stated in its name: an image that serves as the reference for positional alignment of images taken immediately before a treatment fraction delivery. The reference image files often include associated data from the treatment planning process, such as contours and isocenters, that further help orient the patient with respect to the treatment plan. The primary imaging modality to generate reference images is fan beam computed tomography (Benedict 2010). Fan beam systems utilize an x-ray tube to generate a fan of kilovoltage (kV) photons that are incident on a thin row of detectors on the opposite side of the patient.

The second component necessary for IGRT is the localization image. The localization image, obtained immediately prior to the delivery of a fraction of radiation, is aligned to the coordinates of the reference image to direct the beam. Once the patient is initially immobilized on the treatment table in the same way as during the reference image and planning process,

localization images are acquired. Generating localization images can be accomplished with various imaging systems in 2D or 3D (Lovelock 2005, Purdie 2007).

The final component to IGRT is image registration. Registration is the alignment or fusion of the localization image to the reference image to determine the difference between patient and target positions. Registration is typically performed in software displaying the reference image and localization images overlaid on each other. Which can be seen in Figure 1.2.

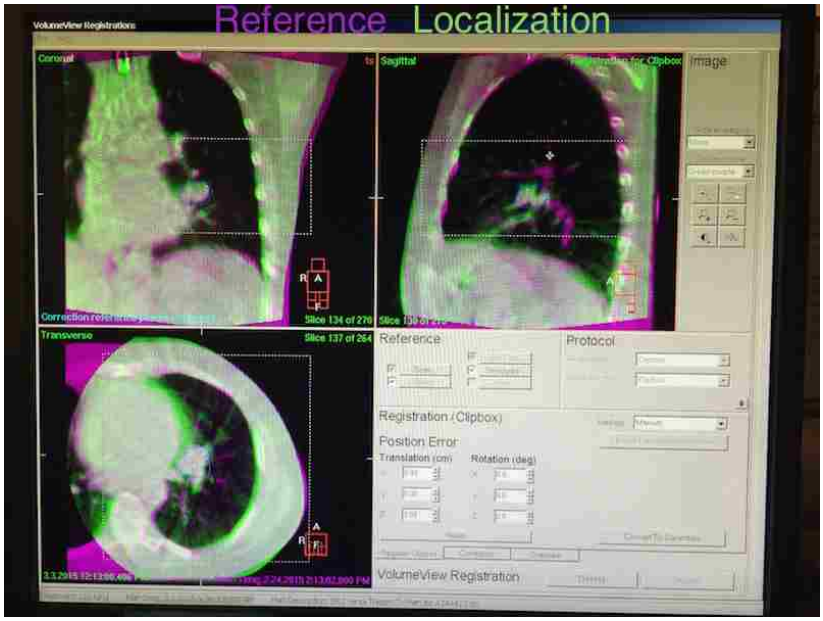

Figure 1.2: Example of image registration software. The purple represents the reference image, the green represents the localization image.

Figure 1.2 shows a screenshot of image registration software with the reference scan colored purple overlaid on the localization scan colored green. The registration can be performed manually or automatically with algorithms (Yin 2009). Two algorithms are frequently used for image registration in IGRT. The first is the chamfer algorithm, which matches edge information between two image sets in a designated area or volume (Lu 2010). This method focuses on

matching bones, because they offer the sharpest changes in density in the body creating clear edges in images (Sykes 2009). The second algorithm is the cross correlation method. The cross correlation method matches pixel or voxel grey-scale intensity values throughout a user designated area or volume (Hill 2001). In addition to edge information, the cross correlation method includes the matching of soft tissues in images (Lu 2010, Barber 2014).

1.3 FAN BEAM AND CONE BEAM COMPUTED TOMOGRAPHY

Lung SBRT uses two imaging modalities in its IGRT process. The preferred modalities for reference and localization image generation are fan beam computed tomography and cone beam computed tomography, respectively (Groh 2002, Benedict 2010). The two systems operate under the same basic principles of image reconstruction but differ in their geometries.

Fan beam computed tomography generates an image by rotating a kilovoltage (kV) fan radiation source around a patient several times and recording the photons that pass through and to reach the detector, visually demonstrated in Figure 1.3a. This creates very thin 1 dimensional (1D) projections of photon transmission through a thin slice of the patient that are reconstructed by filtered backprojection algorithms into a 2 dimensional (2D) cross sectional slice of a patient. With several rotations around the patient along the superior-inferior (SI) axis, 2D slices can be combined to create a 3 dimensional (3D) image of the patient. To reduce scan time, 1D projections are collected helically as the patient slowly passes through the rotating fan of x-rays. This method of computed tomography is referred to as 3D helical CT.

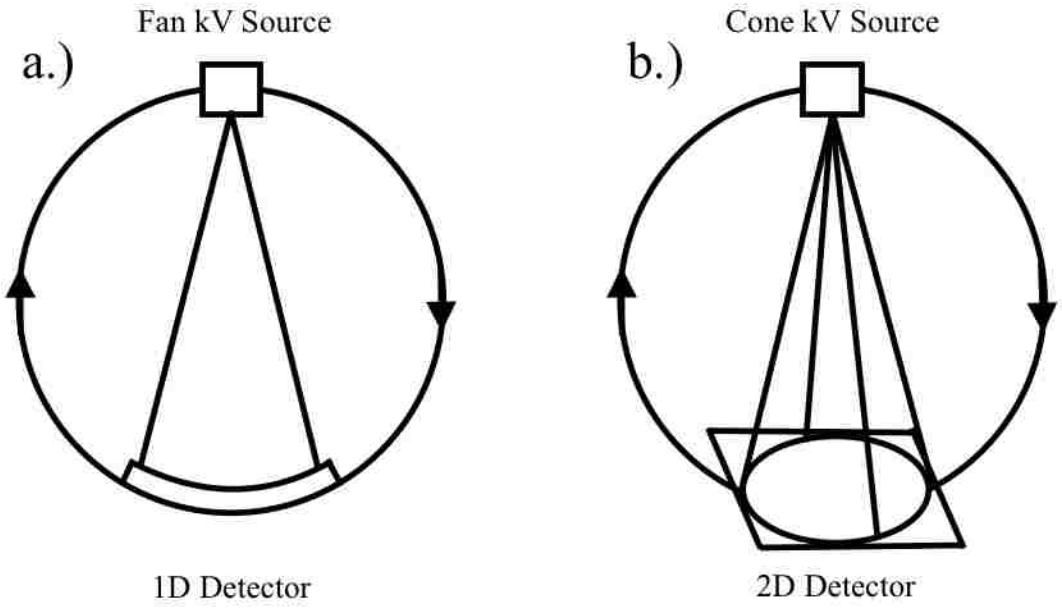

Figure 1.3: a.) Fan beam computed tomography geometrical set up; b.) Cone beam computed tomography geometrical set up.

Cone beam computed tomography generates an image by rotating a kV cone radiation source around a patient a single time and recording the photons that pass through and to reach the detector, visually demonstrated in Figure 1.3b. Instead of the fan beam and narrow detector in 3D helical CT illustrated in Figure 1.3.a, cone beam computed tomography utilizes a cone of kV radiation and a flat panel amorphous silicon detector to collect projection data, shown in Figure 1.3.b. This method is referred to as 3D CBCT. 3D CBCT records projection data in 2D instead of 1D. Computer software uses a Feldkamp-Davis-Kress filtered backprojection algorithm to reconstruct a 3D image from the 2D projections collected with cone geometry.

For IGRT, a cone beam system is attached to the linac gantry such that the 3D CBCT system is oriented orthogonal the treatment beam. This gantry set up is shown in Figure 1.4.

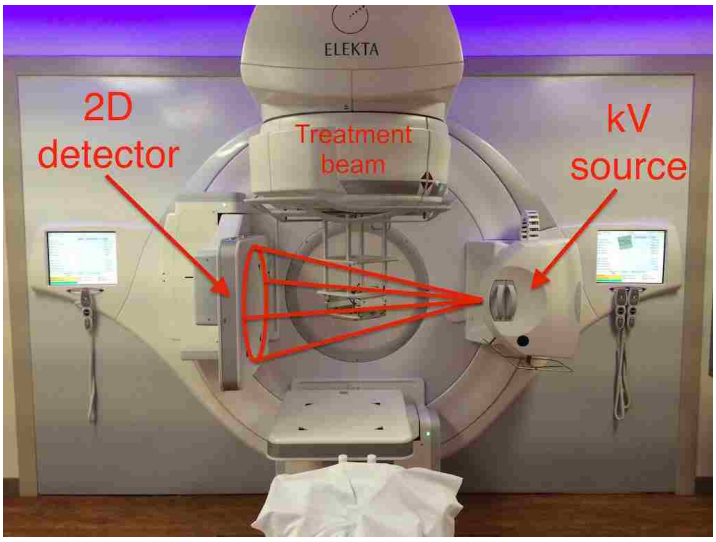

Figure 1.4: kV x-ray tube and kV detector panel for the generation of 3D CBCT images mounted orthogonal treatment beam.

3D CBCT is increasingly being implemented in the localization of tumors in the lung for SBRT (Borst 2007). In lung SBRT patients, 3D CBCT is a useful tool for localization with alignment errors of less than 2 mm (Purdie 2007, Wang 2013). Although 3D CBCT has small errors in localization, the slow nature of the data acquisition causes moving objects in 3D CBCT to average over their range of motion in the final 3D image, creating blurred volumes.

1.4 RESPIRATORY MOTION MANAGEMENT IN FAN BEAM AND CONE BEAM COMPUTED TOMOGRAPHY

Patient and target motion caused by respiration is a large source of error in visualization and localization of moving targets in both 3D helical CT and 3D CBCT (Keall 2006). The effect of regular target motion due to respiration during 3D helical CT is demonstrated in the scans of a sphere stationary and moving periodically in the direction of table motion, shown in Figure 1.5. The appearance of multiple sections of the sphere in different locations is a result of interplay effects between the advancing scan plane and the direction of target motion (Rietzel 2005)

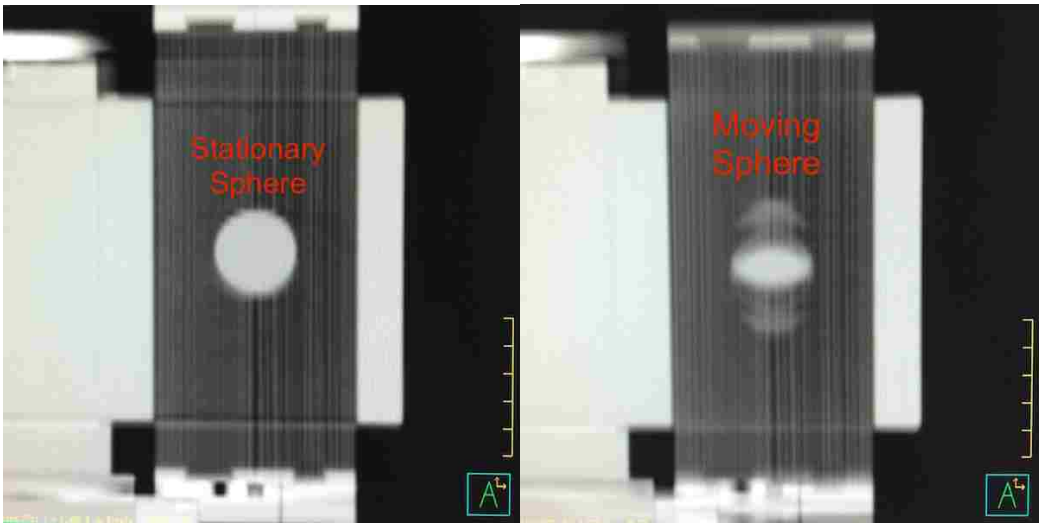

Figure 1.5: Left: 3D helical CT of a stationary sphere. Right: 3D helical CT of the same sphere moving periodically.

In order to reduce these artifacts, time resolved 3D helical CT (4D CT) was developed to show the motion in multiple independent 3D images. 4D CT uses an external system to record the movement of a surrogate for respiratory motion, often the anterior-posterior motion of the abdomen, during the collection of multiple 1D projection images. Recording of the respiratory trace is performed with an infrared CCD camera that tracks the movement of a reflector box on the patient's abdomen. 4D CT collects data in a cine, "step and shoot" fashion instead of helical. The scanner images multiple slices for a user-specified duration (approximately 1-1.5 sec longer than the average breathing period of the patient) then moves to the next table position, imaging the next group of slices of the patient. This scan, along with the respiratory trace file are pushed to the 4D vendor software for retrospective binning and reconstruction. 4D CT software sorts the 1D projections into time bins according to the phase of the breathing cycle during which they were recorded. These 4D CT software systems reconstruct multiple images displaying the internal anatomy at different times in the patient's breathing (Rietzel 2005, Langner 2010). An example of one such 4D CT software system is shown in Figure 1.6.

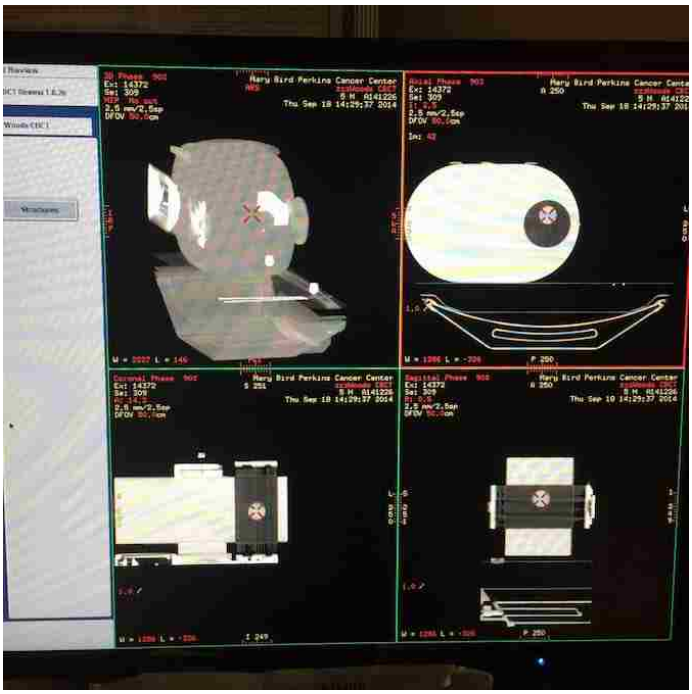

Figure 1.6: Screenshot of a single 3D phase image in 4D CT software.

4D CT software typically creates 2 to 10 individual 3D images corresponding to different phases in the respiratory motion. 4D CT programs produce images corresponding to single phases such as peak inhale or exhale, as well as use the multiple phase images to create composite 3D image datasets. Two 3D image datasets that can be created by 4D CT systems are maximum intensity projections (MIP) and average intensity projections (AIP). Selecting the maximum intensity value for a pixel location across every slice creates the MIP, which is only used for the delineation of the ITV during planning (Wang 2007). Averaging all intensity values for a pixel location from every slice creates an average intensity projection (AIP), which has been reported to be a useful reference image for 3D CBCT localization images (Hugo 2007).

3D CBCT scanners exhibit motion artifacts that differ from 3D helical CT but can still degrade image quality. Periodic motion results in blurring of objects in 3D CBCT, but less complex than interplay effects in 3D helical CT (Song 2009). Periodic respiration isn't

sinusoidal, with a tendency to spend more time exhaling than inhaling. This disparity causes fewer 2D projection images to span the inhale phase in reconstruction. An increase in the time spent at inhale leads to lower contrast and underestimated target volumes in the 3D CBCT for clinically representative phantoms and patients. Underestimation of the target at one extreme in 3D CBCT can lead to errors in localization through incorrect registration of the target volume to the radiation field (Vergalasova 2011). The 4D projection binning techniques implemented for 3D helical CT can also be applied for respiratory correlation in 3D CBCT.

An alternative process for respiratory correlated 3D CBCT (4D CBCT) sorts the 2D cone beam projections into independent phase bins (Sonke 2005). Given the 2D nature of cone beam projection data, the breathing signal can be extracted from moving internal structures, removing the need for external respiratory recording systems utilized in 4D CT (Zijp 2004).

The extraction of the respiratory trace by this method is a multistep process. The first step is slowing the gantry rotation; to have enough 2D projections to reconstruct multiple 3D images of the same volume at different times in a respiratory cycle, the gantry speed is slowed to 1/4 of the speed of 3D CBCT, with a scan time of approximately 4 minutes compared to 1 minute for 3D CBCT.

In the second step each individual projection is processed enhance edges, including the diaphragm (shown on the left side of Figure 1.7). Each enhanced 2D image is then projected onto the SI axis (shown on the right side of Figure 1.7).

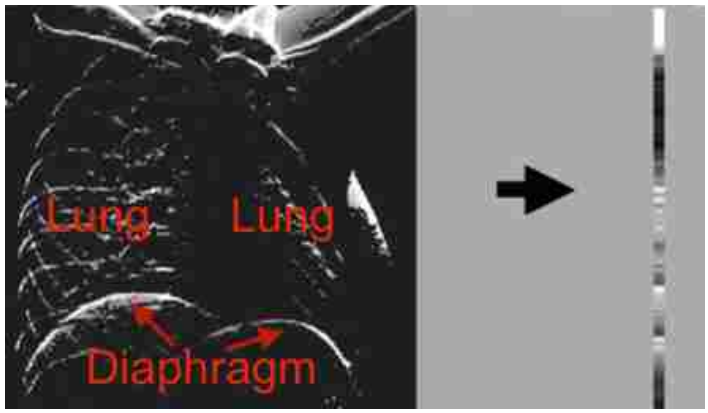

Figure 1.7: (Left) Enhanced 2D cone beam x-ray image with the diaphragm visible at the bottom and (right) the projection of the 2D image onto the SI axis (right) (Zijp 2004).

All the 1D SI projections are then combined and displayed as a 2D image dubbed the "Amsterdam Shroud" (Figure 1.8). The algorithm does not try to isolate the diaphragm but relies on the fact that it is the only feature that moves periodically, clearly seen at the bottom of the shroud.

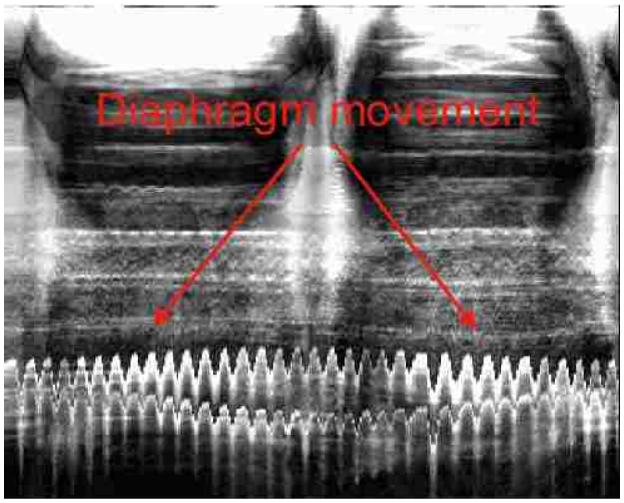

Figure 1.8: The Amsterdam shroud (Zijp 2004)

After more image processing, the area of the shroud with the most temporal variation (the diaphragm) is extracted and the patient's respiratory motion is recorded. The respiratory record

then guides retrospective binning of the 2D cone beam projections and they are reconstructed into independent phase bins.

Recent commercialization of the 4D CBCT process described (Symmetry™, Elekta Ltd., Crawley, West Sussex, United Kingdom) has made the modality available for use in IGRT. The availability of 4D methods in reference and localization scans has created a multitude of possible combinations for image guidance in lung SBRT. The appropriate choices of planning and reference image options than can reduce the PTV compared to 3D helical CT. Current techniques are displayed visually in Figure 1.9.

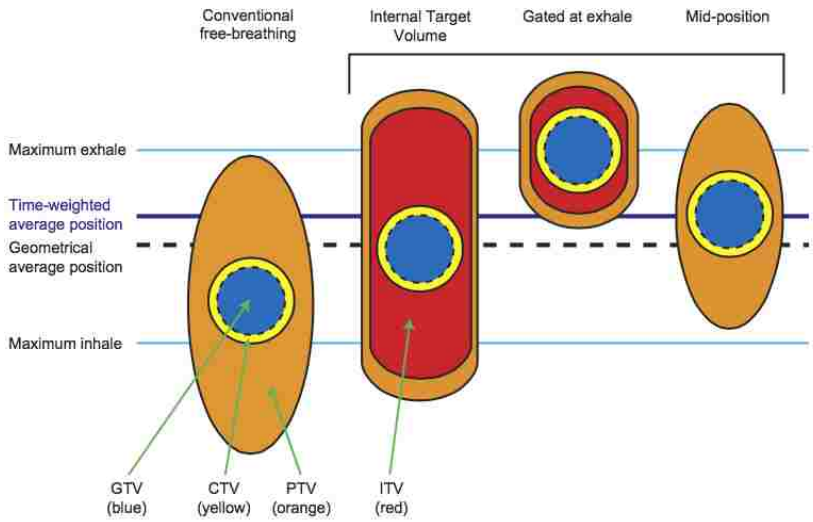

Figure 1.9: Examples of different treatment planning concepts made available by 4D CT: The ITV, exhale gating, and mid-position. The traditional PTV derived from 3D helical CT is shown on the left. (Wolthaus 2008).

These options include the contouring of a MIP to generate an ITV encompassing the tumor motion overlaid on a 3D helical CT, an exhale phase image of a target for gated radiotherapy, and a target mid-position image (time-based average position) (Guckenberger

2009). The methods derived from 4D CT have been shown to have similar treatment outcomes with the use of online soft tissue localization (Wolthaus 2008).

The originators of 4D CBCT advocate for the use of the time based mid-position image from 4D CT reconstruction as a reference for image guidance (Sonke 2009). 4D CBCT registered to a mid-position can perform alignments for lung SBRT with errors less than 1.5 mm. The accurate creation of a mid-position image as a reference is currently unavailable in commercially available software, limiting its use to institutions that generate in-house methods to create them. As an alternative, the ITV contour generated from a MIP was been successfully used with 4D CBCT for the image guided treatment of multiple metastases in the lung (Li 2006). Additional implementations of 4D CT information coupled with 4D CBCT have shown improvements over 3D CBCT.

In patients, the use of 4D CBCT registered to an inhale phase from 4D CT had errors of 1.5 mm in alignment of lung targets compared to 1 mm for the alignment of a 3D CBCT to an AIP (Hugo 2007). The use of the inhale phase as reference for 4D CBCT did not provide as much as an advantage over 3D CBCT as the use of exhale phase imagery. The exhale phase from 4D CBCT registered to the exhale phase from 4D CT provided improvements in alignment of 3.6 mm and 1.9 mm compared to 3D CBCT registered to an ITV and 3D CBCT registered to the exhale phase from 4D CT, respectively (Sweeney 2012).

In simple rubber ball phantoms moving regularly, with short pauses corresponding to an exhale location, the range of motion in 4D CBCT was shown to agree with 4D CT (Hugo 2007). Implementation of 4D CBCT allowed for the study of respiratory motion characteristics, such as target volume and motion amplitude, of patient tumors throughout lung SBRT treatments instead of only at 4D CT planning. Comparisons of tumor motion characteristics in 4D CBCT, such as

amplitude of motion across SBRT fractions, was found to be reproducible over all fractions, but single fractions observed amplitude increases of up to 10 mm in some patients (Purdie 2006, Bissonnette 2009). These findings are contrary to MRI measurements throughout SBRT that show increased GTV sizes in all patients undergoing lung SBRT, attributed to an increase in tumor motion amplitude, tumor size, or both. 3D CBCT measurements of motion amplitude showed both increased and decreased motion amplitude up to 8 mm (Guckenberger 2007). All findings on lung tumor behavioral changes concerning the range of motion or target dimensions during SBRT agreed that changes between fractions can occur, the magnitude and direction of which were largely patient dependent. The effect of changes in respiratory amplitude on the error in localization remains unknown for 3D CBCT and 4D CBCT image guidance.

1.5 MOTIVATION FOR RESEARCH

Prior studies have shown that 4D-CBCT has benefits over other methods for image guidance; however, there are gaps in the current body of knowledge. First, all previous studies discussed the use of 4D-CBCT on patients, where the true extent of the tumor motion amplitude and the size of the tumor are unknown. Patient studies can only compare the constancy of these tumor aspects across multiple imaging studies since none can be assumed to be “ground truth”. For those studies that have utilized a phantom for 4D CBCT research, non-sinusoidal respiratory waves have been used, but the phantom was not representative of the clinical case. No study on 4D-CBCT has compared absolute values of tumor amplitude and size in a clinically representative phantom.

Second, the impact of the choice of reference image is unknown. The current 4D CBCT system was designed specifically to use a time based mid-position image calculated from 4D CT as its reference image; however, accurate generation of such a frame is not commercially

available. Although several reference images have been used for 3D to 4D comparisons, there has yet to be a study that compares different types of reference images that can be used for the 3D to 4D comparison, with the goal of determining which provides the most accurate localization.

Lastly, the impact of changes in a tumor's size and amplitude of motion throughout lung SBRT fractions remains unknown. Several investigations into these changes showed they are largely patient dependent, but no studies have examined how these potential changes in the respiratory tumor motion amplitude between planning and treatment will affect 3D CBCT and 4D CBCT localization.

1.6 HYPOTHESIS AND SPECIFIC AIMS

The hypothesis of this study was that the use of 4D CBCT allows a user to measure the amplitude of tumor motion more accurately than 3D CBCT. Also, 4D CBCT will allow for the measurement of a tumor's diameter at its exhale phase in agreement with reality. Additionally it was hypothesized that the use of the exhale frame from 4D CBCT registered to the exhale phase from 4D CT would provide statistically significant reduction in localization error compared to other 3D CBCT and 4D CBCT guidance methods. Lastly, it was hypothesized that 4D CBCT would provide a reduction in localization error compared to 3D CBCT when patient respiratory motion amplitude changes with respect to the motion at treatment planning.

To test these hypotheses, three specific aims were completed as follows:

Aim 1: Measure the amplitude of motion in 3D CBCT and 4D CBCT and the size of the tumor at its exhale phase from 4D CBCT. Compare these measurements to the known tumor size and motion amplitude in a clinically representative phantom. The goal of this specific aim was to determine which type of localization (3D CBCT or 4D CBCT) image could most accurately

measure the amplitude of tumor motion in clinically representative phantom driven by patient respiratory traces.

Aim 2: Determine the optimal combination of reference image, localization scan type, and registration method. Multiple combinations of reference images, localization scans, and registration types (called “image guidance methods” collectively) with repeat scans at multiple known offsets were examined to determine which method produced the smallest error in localization over all amplitudes and respiratory waveforms.

Aim 3: Determine which image guidance method was the least sensitive to changes in respiratory motion amplitude.

CHAPTER 2: METHODS AND MATERIALS

2.1 DYNAMIC RESPIRATORY MOTION PHANTOM

A dynamic respiratory phantom (Quasar Programmable Respiratory Phantom, Modus Medical Devices Ltd., London, ON, Canada) was utilized for this study (Figure 2.1). The phantom was intended to provide a realistic approximation of a breathing patient with a tumor in both density and motion. The assembly consisted of an acrylic body and a drive unit attached in the center of the body of the phantom. There is an additional cut through the body offset from the center for a model lung insert. Fiducials on the sides, top, and along the centerline of wooden lung insert on the body of the phantom serve to align the it to the multiple imaging systems used throughout the image guidance process.

Figure 2.1: Dynamic respiratory motion phantom implemented for this study.

Various inserts can be attached to the drive motor and moved to mimic tumor motion. The insert used in this project was a split cedar offset lung tumor insert (Figure 2.2). Lung tissue was approximated using cedar because of its similar properties to lung in a CT image. The cedar insert was split, and contains a 3 cm diameter plastic sphere. Isocenter was designated as the center of the extent of motion of the sphere in the lung insert. Table 2.1 shows measurements of the CT number and density for the lung insert materials and actual patient lungs and tumors.

Figure 2.2: Split offset cedar lung tumor insert.

Table 2.1: Measured CT numbers and densities of the lung tumor insert compared to actual patient lungs and tumors.

Material	CT Number	Density (g/cm^3)
Cedar	290-400	0.35
Lung	140-320	0.40
Sphere	~950	0.98
Tumor	~1000	1.05

The phantom simulated respiratory motion by moving the insert in the SI direction, which is coupled to a platform that moves in the AP direction allowing for 4D CT respiratory trace recording. The dynamic nature of the phantom lies in its ability to import and run patient-specific respiratory motion traces previously recorded during 4D CT acquisition. Software loads data points corresponding to physical respiratory motion data over time and uses these values to operate the drive cylinder. Once imported, the software offers editing of the patient respiratory waveforms in the form of amplitude adjustment, frequency adjustment, and simple exponential filters for smoothing irregularities in the trace. An example of a patient respiratory waveform imported into the phantom software is displayed in Figure 2.3.

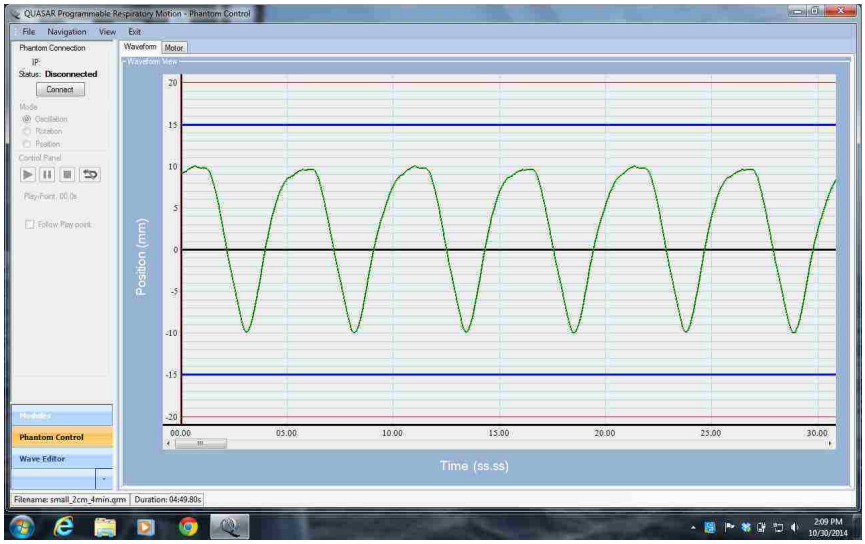

Figure 2.3: Phantom control software showing an imported patient respiratory waveform.

2.1.1 PATIENT-SPECIFIC RESPIRATORY MOTION MODELS

Patient-specific respiratory motion models were used to generate clinically representative images. Characteristics modeled were the amount of time the tumor spent at exhale and the

amplitude of tumor motion. The metric used to quantify the amount of time a tumor spent at exhale was the inspiration to expiration ratio (I/E ratio) (Vergalasova, Maurer et al. 2011). This was defined as the ratio of the number of points that were within 25% of the peak inhale and exhale portions of the respiratory trace. For example, a calculated I/E ratio of 0.5 means the tumor spent twice as much time within 25% of the peak exhale location than within 25% of the peak inhale location.

Patient traces were examined from the archive at MBPCC dating back to 2006. Traces were selected where: the amplitude of motion was consistent across multiple respiratory cycles and the length of consecutive breaths was the same. Three traces were selected that exhibited different I/E ratios, with a fourth irregular trace that did not exhibit the criteria for comparison. Each trace was processed a single time with a low pass exponential moving-average filter to smooth out noise in the respiratory trace. The 4 traces are displayed in Figures 2.4-7.

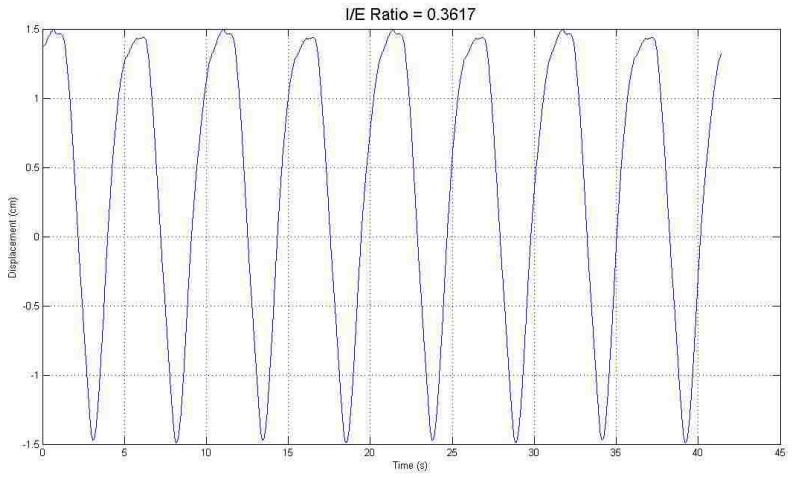

Figure 2.4: Patient respiratory model with the longest pause at exhale, I/E ratio = 0.3617.

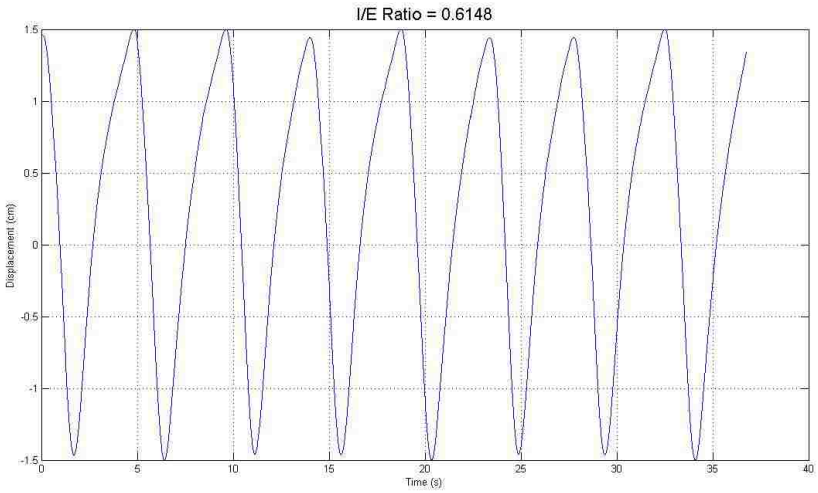

Figure 2.5: Patient respiratory model with an intermediate pause at exhale, I/E ratio = 0.6148.

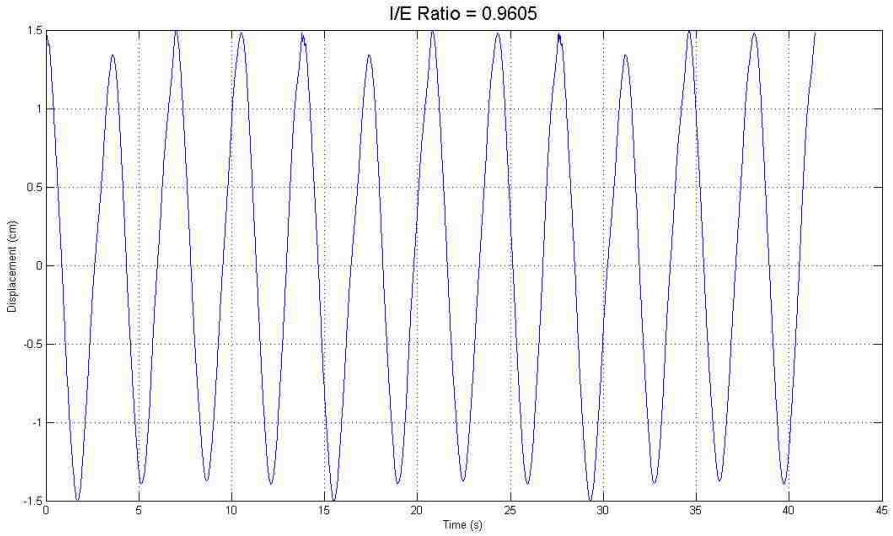

Figure 2.6: Patient respiratory model with the shortest pause at exhale, I/E ratio = 0.9605.

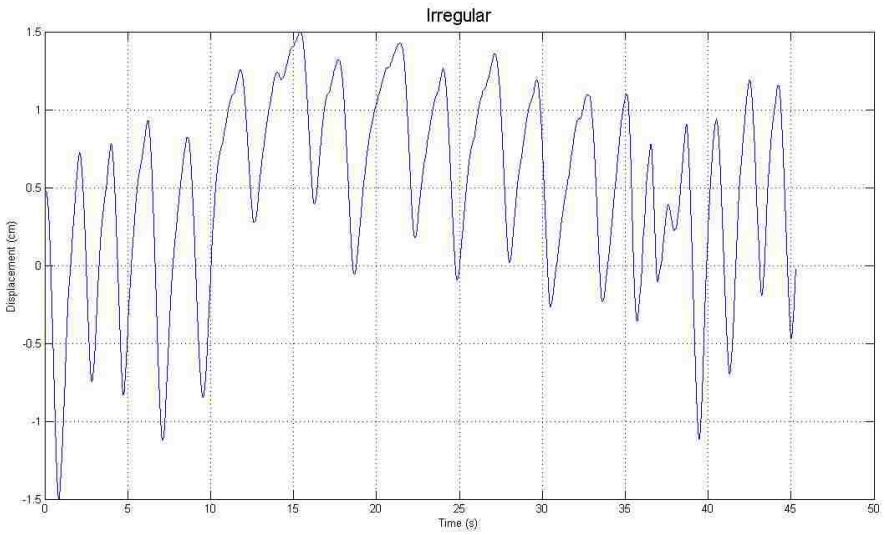

Figure 2.7: Irregular trace exhibiting none of the criteria for selection.

Amplitudes of 1 cm and 2 cm were used for each respiratory trace. Each I/E ratio waveform was used with each amplitude for this study, except for the irregular case that was only run with the larger 2 cm amplitude. The 1 cm and 2 cm motion amplitudes were also adjusted by ±30% at localization to simulate changes in respiratory motion amplitude. These additional amplitudes were used to bolster the data in Aim 1 and were essential to Aim 3. Table 2.2 shows amplitudes of motion used throughout the study and the corresponding aims they were used for.

Table 2.2: Amplitudes of motion used in this study and the Aims they were used for.

Amplitude of Motion	Aim
0.7 cm	1,3
1 cm	1,2,3
1.3 cm	1,3
1.4 cm	1,3
2 cm	1,2,3
2.6 cm	1,3

2.2 AIM 1, MEASUREMENT OF MOTION AMPLITUDE AND TUMOR SIZE

3D CBCT and 4D CBCT localization images were acquired on a clinical linear accelerator with a gantry-mounted CBCT system and image guidance software (Elekta Versa HD, X-ray volume imager (XVI), Elekta Ltd. Crawley, West Sussex, United Kingdom). The phantom was positioned on the treatment couch and its fiducial markers were aligned to the external laser system in the treatment vault. Image acquisition parameters for the 3D CBCT and 4D CBCT scans are listed in Table 2.3.

Table 2.3: Image acquisition parameters for 3D CBCT and 4D CBCT.

Scan	Arc	Gantry Speed	Time	Tube Potential	Tube Current	Projections	Filter	Collimator
3D CBCT	360°	270°/min	1 1/3 min	120 kV	422.4 mAs	660	F1	M20
4D CBCT	200°	50°/min	4 min	120 kV	422.4 mAs	1320	F0	S20

From these images, respiratory amplitude and tumor size were measured for all 7 amplitudes listed in Table 2.2. In the 3D CBCT images, the amplitude was measured with the length of the blurred tumor on the image. This was performed from the measuring tool provided in the image acquisition software. The two points for measurement were chosen at the opposite edges of the 3D blur, defined as the nearest pixels to the 50% change in pixel values of the blurred sphere relative to the surrounding cedar (Figure 2.8).

In the CBCT software, the window and level of the 3D CBCT image was 650 and 491, respectively, for measurement. These were chosen for the best definition of the sphere edges as well as surrounding “soft tissue” (cedar) in each image acquisition. In the 4D CBCT images, the amplitude was automatically calculated and displayed by the software (Figure 2.9). Additionally,

an AIP was generated from the 4D CBCT and the amplitude was measured using the same methodology as the 3D CBCT blur measurement.

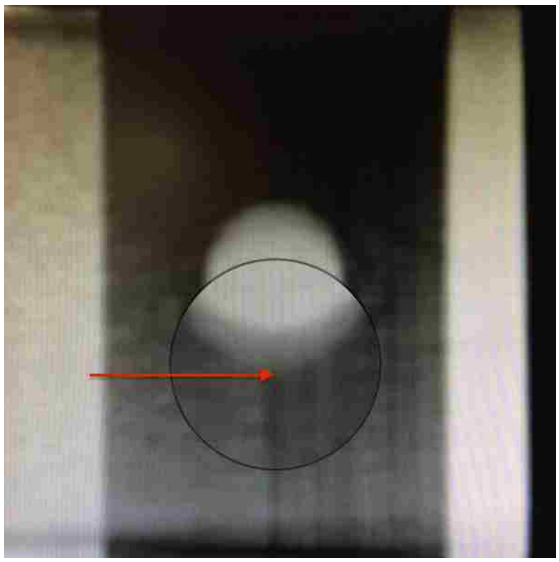

Figure 2.8: Red arrow points to 50% change in pixel values of the blurred sphere relative to the surrounding cedar used for measurement of the amplitude.

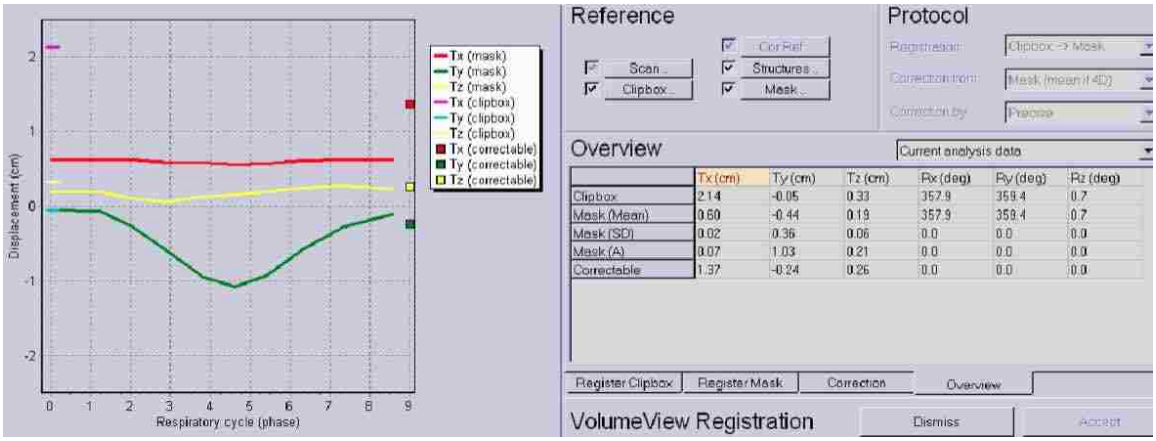

Figure 2.9: 4D CBCT software showing displacement (i.e. amplitude of motion) of the target in all directions.

15 3D CBCT and 4D CBCT images were acquired each patient model, totaling 210 images. For multiple acquisitions at each experimental condition, results were averaged. Tumor size and motion amplitude were intercompared for the 3 datasets (3D CBCT, 4D CBCT, and AIP from 4D CBCT), resulting in 3 comparisons for each I/E ratio and amplitude. Student's t-test (two-tailed) for independent samples was used to determine if the differences between the localization methods were statistically significant. For a significance level of 0.05 with Bonferroni's correction of 3 for the number of inter-comparisons, the target p-value to indicate significance was 0.017.

Tumor size was measured on the exhale frame of the 4D CBCT images. The exhale frame was chosen because it provided the best visualization of the moving sphere. The same method of finding the 50% change between the cedar pixel values and the pixel values of the sphere was used to determine measurement points. The measurement was performed along the direction of motion (SI) axis.

2.3 AIM 2, LOCALIZATION ERROR OF 3D AND 4D CBCT FOR UNCHANGED PATIENT RESPIRATORY BEHAVIOR

The purpose of this specific aim was to quantify the error in localization of multiple techniques tested for both 3D CBCT and 4D CBCT localization with the goal of determining the combination of reference image, localization scan, and registration technique that minimizes this error when the respiratory motion amplitude remains unchanged throughout. The rationale behind this comparison was to identify the best choice of reference images derived from 4D CT.

2.3.1 REFERENCE IMAGE ACQUISITION

Every localization image that is acquired must be compared with a reference image to determine how the image object should be shifted for proper positioning. In this study, 3

reference images were examined for each patient model: a 3D helical CT, an exhale phase from 4D CT, and an AIP from 4D CT. All reference images were acquired using a 16-slice CT scanner (LightSpeed RT, General Electric Healthcare, Fairfield, Connecticut, U.S.) equipped with respiratory binning software (Advantage 4D, General Electric Healthcare, Fairfield, Connecticut, U.S.) for 4D CT. Respiratory traces were generated using a CCD-based external fiducial tracking system (Real-Time Positioning (RPM), Varian Medical Systems, Palo Alto, California, U.S.). This tracking system included a box with circular reflective spots, an infrared CCD camera, an infrared light source, and recording software.

Prior to image acquisition, the phantom was aligned to the external room lasers in the CT suite using the isocenter marks on the phantom. After the phantom was aligned, the reflector box was placed on the anterior-posterior motion platform of the respiratory phantom. The camera was adjusted such that the reflective box was centered in the frame, as seen in Figure 2.10.

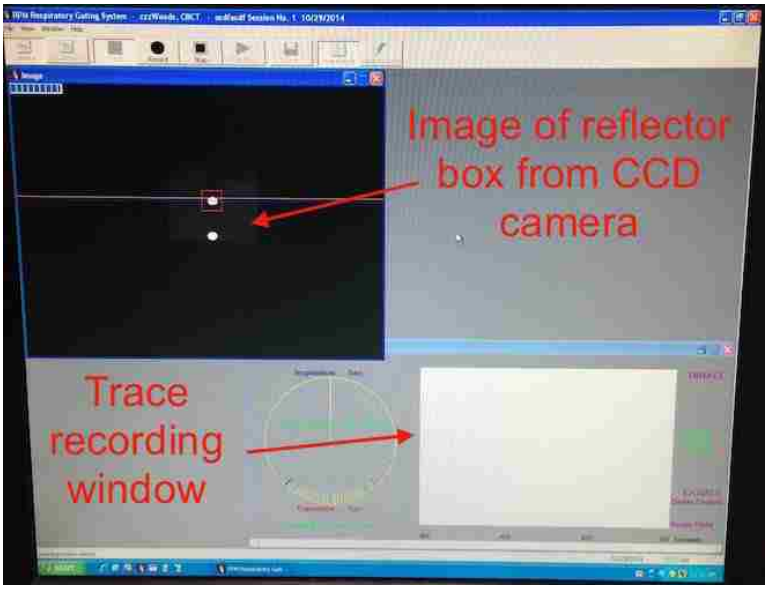

Figure 2.10: Software for the recording of abdominal respiratory motion by infrared imaging of reflective spots.

To complete the set-up, the phantom was plugged into a power source and the desired waveform was loaded using the phantom software. Once the phantom set-up was complete, basic patient data was entered into the CT scanner control computer. The imaging protocol used for all CT image acquisitions of lung SBRT treatments was the "4D Gating" preset from the vendor. It included 2 scans: a 3D helical CT scan and a 3D cine CT scan. The image acquisition parameters are listed in Table 2.4.

Table 2.4: Image acquisition parameters for reference image generation.

Scan	Tube Potential	Tube Current	Pitch	Slices	Slice Thickness	Scan Length
3D helical CT	120 kV	400 mAs	0.562	80	2.5 mm	20 cm
3D cine CT	120 kV	400 mAs	N/A	80	2.5 mm	20 cm

Once these scans were complete, the 3D helical CT images were pushed directly to the treatment planning system (Pinnacle3, Fitchburg, Wisconsin, U.S.). As an example, a 3D helical CT image of the phantom running the Small I/E ratio respiratory trace operating at 1 cm amplitude is shown in Figure 2.11.

The 3D cine CT image was acquired in conjunction with respiratory trace recording. The 3D cine scan uses no pitch because of the step and shoot delivery of radiation. The cine scan duration per slice was set to approximately 1-1.5 sec longer than the average breathing period of the patient. The scanning time is dependent on the breathing duration of the patient, and was slightly different for each waveform in this study, ranging from 5.5 sec to 6.5 sec. This cine scan, along with the respiratory trace file, were pushed to the vendor software (Figure 2.12) for retrospective binning and reconstruction into the 4D CT dataset.

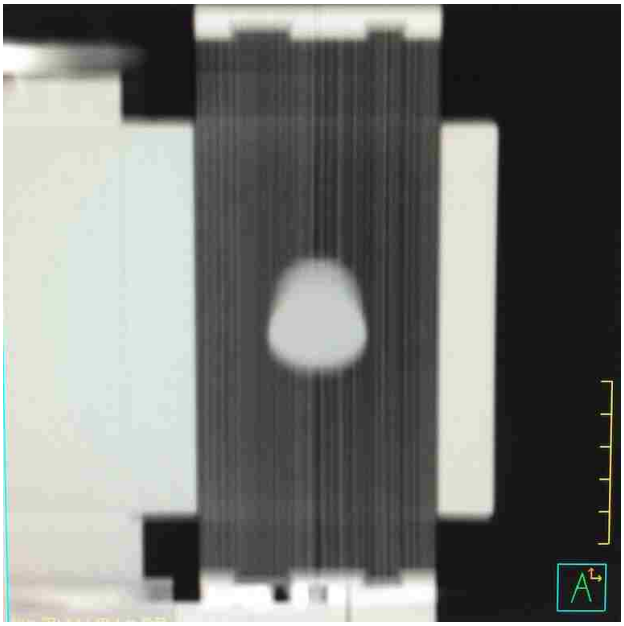

Figure 2.11: 3D helical CT image of the dynamic respiratory phantom moving with the 10 mm, Small I/E ratio respiratory motion trace.

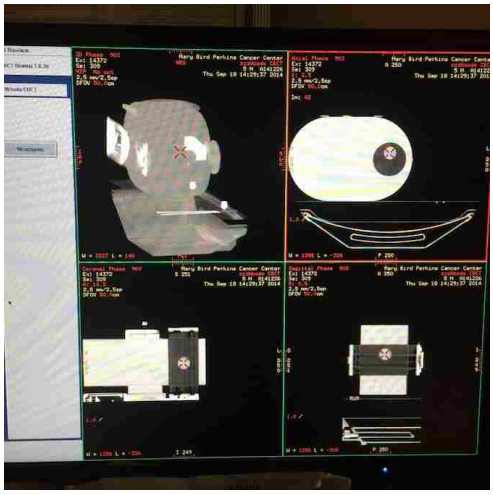

Figure 2.12: Three orthogonal views of a single phase of 4D CT reconstruction and a 3D rendering of the phantom (top left).

The 4D CT reconstruction application, seen in Figure 2.12, was based on retrospective gating CT application software that used an associated respiratory trace and the 3D cine CT

images to generate a series of images correlated to various phases in a patient's breathing pattern. There were several customizable features that could be adjusted for 4D reconstruction. The 4D CBCT imaging system by default generated 10 bins of respiratory phases, so this was chosen for 4D CT reconstruction. After reconstruction, the 4D CT data was pushed to the TPS.

From the reconstructed 4D CT, two additional reference images were generated and exported to the TPS: the exhale phase and the AIP. The exhale phase corresponded to the tumor's maximum exhale position among the 10 phase bins. The exhale phase image for the 10 mm, Small I/E ratio trace is shown in Figure 2.13. The exhale phase was chosen as the image where the tumor was located at the most superior position. This position was typically the 50% or 60% point in the motion period of the tumor, which depended on the waveform used, excluding the irregular waveform, for which the 70% phase bin was selected. This difference between waveforms was due to the different extent of pause at exhale between the multiple waveforms chosen for the study. Table 2.5 displays the phases chosen for the reference image for each patient model.

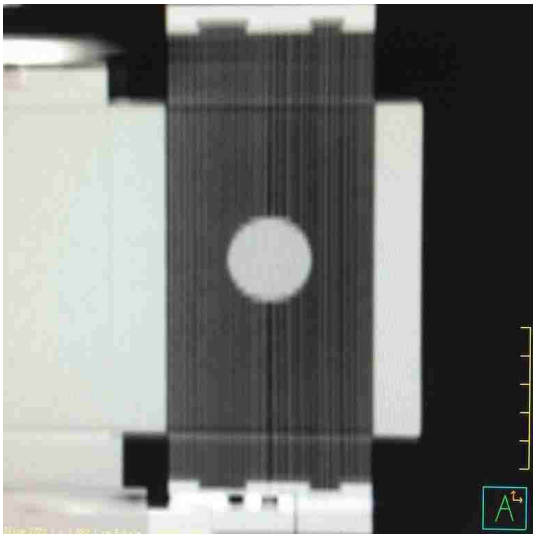

Figure 2.13: Exhale phase image of the dynamic respiratory phantom moving with the 10 mm, Small I/E ratio respiratory motion trace.

Table 2.5: Exhale phases for corresponding patient models.

Patient Model	Exhale Phase
Small I/E	60%
Medium I/E	50%
Large I/E	50%
Irregular	70%

The final reference image produced was the AIP from the 4D CT. The method for AIP generation was described previously. An example of an AIP used as a reference is shown in Figure 2.14.

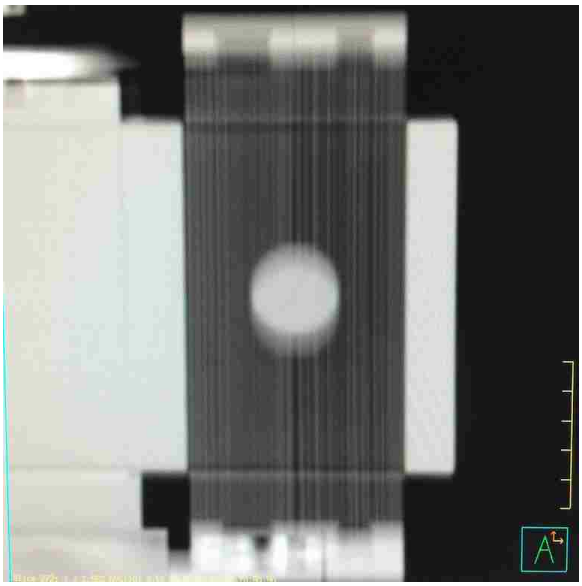

Figure 2.14: AIP of the dynamic respiratory phantom moving with the 10 mm, Small I/E ratio respiratory motion trace.

In summary, three references images were generated: the 3D helical CT scan of the phantom, the exhale phase image from 4D CT, and the AIP from 4D CT. All reference images for all patient models are shown in the Appendix.

2.3.2 TREATMENT PLANNING

Before the reference images were loaded into the image guidance software, the designation of the isocenter and the creation of a contour of the target had to be performed in the TPS. This was necessary because the CBCT localization software required a contour to create a 3D volume within which the registration algorithm attempted to match pixels values between the reference and localization images.

The first step to create plan contours was to indicate to the TPS where the external room lasers were on the phantom during reference image acquisition. The external room lasers in the TPS were displayed as green lines in the software, showing their alignment in 3 different views to the fiducials (Figure 2.15).

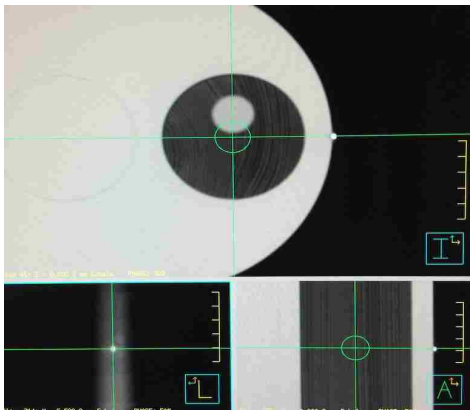

Figure 2.15: Laser localization step in TPS for the designation of isocenter in the reference image.

Next the visible tumor was contoured. For all of the reference images, every value that was larger than the average of expected cedar CT number was contoured. Examples of contours for each reference image are displayed in Figure 2.16. All contours for all patient models are shown in the Appendix.

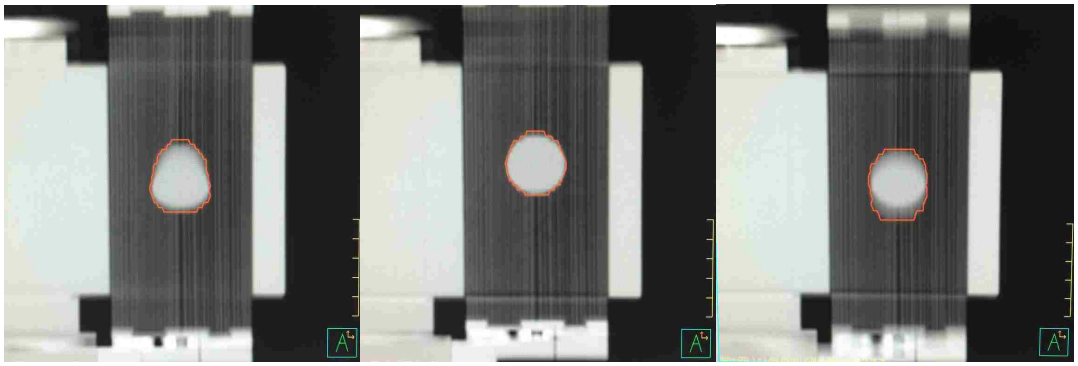

Figure 2.16: Examples of target contours for 3D helical CT (left), exhale (middle), and AIP (right) reference images for the 10 mm, Small I/E patient model.

2.3.3 CBCT ACQUISITION

The phantom was positioned on the treatment table and initially aligned to the external lasers in the treatment room with the isocenter marks used throughout the study. There was a small discrepancy between the external laser isocenter and CBCT imaging isocenter, typically on the order of 1 mm, which required the initial registration of a 3D CBCT image of the static phantom to a 3D helical CT of the static phantom. The CBCT system then shifted the phantom to its imaging isocenter, readying it for data collection.

3D CBCT and 4D CBCT image acquisition, as described in Aim 1, was performed at 5 different locations including isocenter and 4 locations away from isocenter along the axis of motion (SI). These 4 known errors were introduced in the position of the phantom so the registration techniques in the CBCT software could correct them. They consisted of shifts of 2 mm and 5 mm superior to isocenter and 3 mm and 6 mm inferior to isocenter. These offsets were chosen because they represented typical errors experienced in patient set up. At each position, the phantom was scanned 3 times to accumulate good representation of the random errors in the

study. The difference between the physical corrections from the CBCT software and the known shifts away from isocenter was used to quantify the error in localization.

2.3.4 REGISTRATION METHODS

This study compared the manual registration and automatic techniques available with 4D CBCT. Manual registrations were performed using a visual overlay of the CBCT image to align with the reference image in three dimensions. For this study, an experienced radiation therapist performed all manual registrations. For this process, the same window and level for 3D CBCT in Aim 1 were used for consistency; the window and level for the 4D CBCT images were 946 and 634, respectively. These window and level values were chosen to maximize the visibility of the tumor and the surrounding cedar.

Automatic image registration was performed using the cross correlation algorithm in the CBCT software. The designated volume for registration, or mask, was expanded by 1 cm from the contours of the target generated in the TPS (Figure 2.17). Every automatic registration was performed within the volumetric mask.

Automatic registration within the mask was performed 3 different ways in this study, two used for 4D CBCT images and one for 3D CBCT images. One technique for 4D CBCT was automatic registration of exhale frames. The cross correlation algorithm was applied to automatically register the exhale phase of the 4D CBCT to the exhale phase image from 4D CT reconstruction. To perform a registration between the exhale phase in 4D CBCT and the reference exhale 4D CT phase, the selection “Mask (exhale if 4D)” was chosen, which indicated to the CBCT software to only operate within the 1 cm mask previously generated.

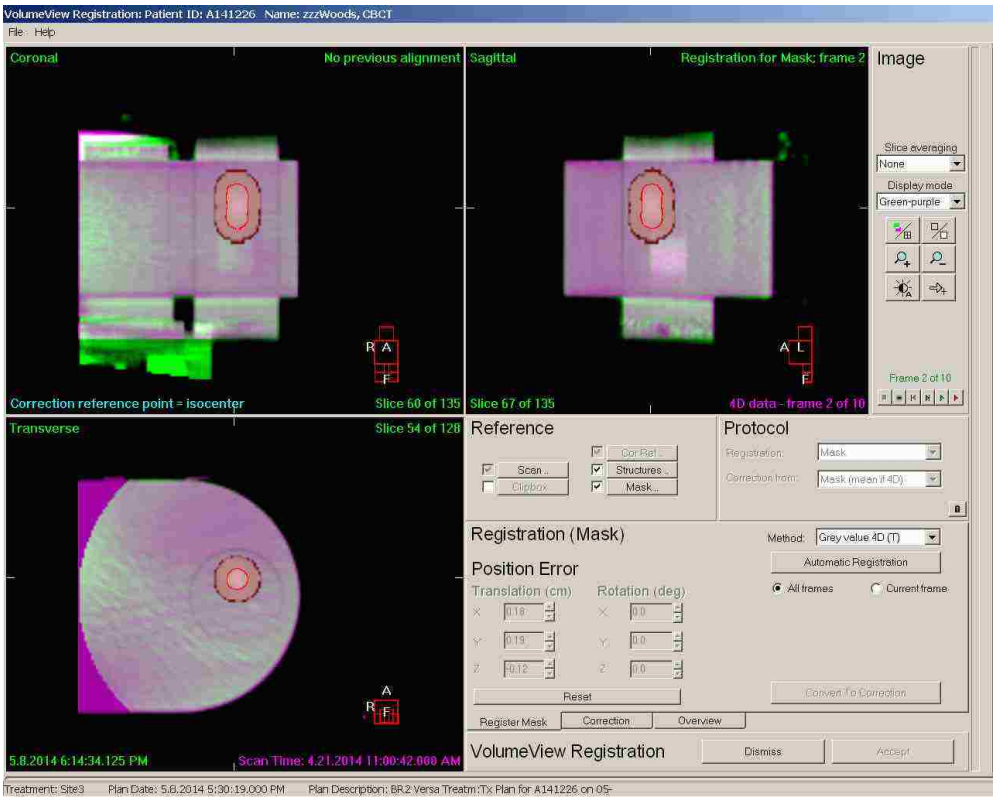

Figure 2.17: Screenshot of CBCT software during automatic registration within a 1 cm generated mask (red area).

The other 4D CBCT automatic registration technique was registration of AIPs. The CBCT system generated an AIP from the 10 phase images. The same cross correlation algorithm was used to register the AIP from the 4D CBCT to the AIP from 4D CT.

The automatic registration technique for 3D CBCT aligned to the AIP from 4D CT. Table 2.6 summarizes each image guidance method used for this study: the pairing of the reference and localization images, as well as the registration method for each. After each registration was complete, the CBCT software reported the physical correction in position to place the phantom back to isocenter.

Table 2.6: Reference images and associated localization types and registration methods. "Automatic" refers to the mask delineated cross correlation registration, either the exhale or AIP from 4D CBCT. "Manual" refers to user alignment with a specified window and level for best view of the target and surrounding tissues.

Image Guidance Method Name	Reference Image	Localization Scan	Registration Method
3D CBCT manual to 3D helical	3D Helical CT	3D CBCT	Manual
4D CBCT manual to 3D helical	3D Helical CT	4D CBCT	Manual
4D CBCT exhale auto to exhale	Exhale from 4D CT	4D CBCT	Automatic Correction from Exhale
4D CBCT exhale manual to exhale	Exhale from 4D CT	4D CBCT	Manual Exhale Frame Alignment
4D CBCT AIP auto to AIP from 4D CT	3D AIP from 4D CT	4D CBCT	Automatic AIP from 4D CBCT to AIP from 4D CT
3D CBCT auto to AIP from 4D CT	3D AIP from 4D CT	3D CBCT	Automatic 3D CBCT to AIP from 4D CT

2.3.5 REPRODUCIBILITY OF PHANTOM SETUP

The accuracy of this study depended in part on the reproducibility with which the user could position the phantom to the imaging isocenter. To quantify the reproducibility, the phantom was then shifted away from isocenter in the SI direction and then realigned to the iscoenter mark. A 3D CBCT of the static phantom was acquired and registered to the 3 helical CT of the static phantom. This process was repeated 5 times in order to measure the reproducibility of phantom alignment before each night of data collection. This process was additionally performed for each of the 4 offsets used in the study to confirm the positioning reproducibility as well.

2.3.6 SUMMARY

As discussed earlier, there were 6 image guidance methods, each of which was investigated for three respiratory traces with 2 amplitudes each, with a fourth irregular trace with a single amplitude. Three scans were performed at each of the 5 phantom locations to have a good representation of the random fluctuations in scanning and localization. The phantom was placed at isocenter, exactly as during the planning scan, and was imaged with offsets in the SI direction to model positioning error. Offsets of 2 mm and 5 mm in the superior direction, and 3 mm and 6 mm in the inferior direction, were used.

2.3.7 STATISTICAL ANALYSIS

The difference between the correction determined by each image guidance method and the known position of the phantom relative to isocenter for each method was the definition of localization error used in this study. These differences were used to test for statistical significance between methods using a generalized linear mixed model. This procedure is referred to as GLIMMIX and it is unique to the commercial statistical analysis software SAS (SAS 9.4, SAS Institute, Cary, North Carolina, U.S.). The GLIMMIX procedure fits statistical models to data with correlations or nonconstant variability and where the response is not necessarily normally distributed. The GLIMMIX procedure assumes normal (Gaussian) random effects in the data. On the condition of these random effects, the data can have any distribution in the exponential family. GLIMMIX required the development of a code that modeled each data point of the study specifically by categorizing each point with its respective combination of image guidance method, patient model, amplitude of motion, and offset from isocenter.

Statistical relationships were calculated with a pairwise least squares means comparison, with a p-value of 0.05. The analysis software reported statistical relationships as letters,

(A,B,C,…). If two calculated averages share the same letter, then any difference between them was not statistically significant. If they did not share the same letter then any difference between them was significant. These relationships were not transitive.

2.4 AIM 3, LOCALIZATION ERROR OF 3D CBCT AND 4D CBCT WITH CHANGES IN PATIENT RESPIRATORY BEHAVIOR

2.4.1 MODELING CHANGES IN RESPIRATORY MOTION

As stated in the background, potential variability exists in patient respiratory behavior. To simulate the behavioral change a patient may experience between fractions, each image guidance method was measured for a respiratory amplitude that was different than the amplitude during planning CT acquisition. The 3D CBCT and 4D CBCT systems were used to align the phantom to isocenter under the conditions of both increased and decreased motion amplitude of the target relative to planning. For the regular I/E ratio planning waveforms, the amplitude was adjusted by ±30% of the original value during localization.

2.4.2 SUMMARY

The 6 image guidance methods previously defined in Aim 2 will be used to localize the same patient respiratory models as Aim 2 but with 30% increased and decreased motion amplitudes during the localization 3D and 4D CBCT scans. The same procedure of multiple scans at offsets and isocenter used in Aim 2 will be implemented again, with the added difference of amplitude changes during localization. 2 additional datasets corresponding to increased and decreased amplitudes will be imported into the same statistical analysis software and undergo a comparison identical to the one performed in Aim 2.

CHAPTER 4: RESULTS AND DISCUSSION

3.1 AIM 1

3.1.1 AMPLITUDE MEASUREMENT RESULTS

Figures 3.1-3.6 show the measurements of amplitude from each localization method compared for each patient model (Small, Medium, and Large I/E ratios). The bar height in each plot corresponds to the average measured amplitude (N = 15). Alphas are shown for each grouping.

Figure 3.1 shows the comparison of the amplitude measurements for each patient model moving with a amplitude of 0.7 cm. Over all patient models, there was a general underestimation of all amplitude measurements from 0.06 – 0.13 cm.

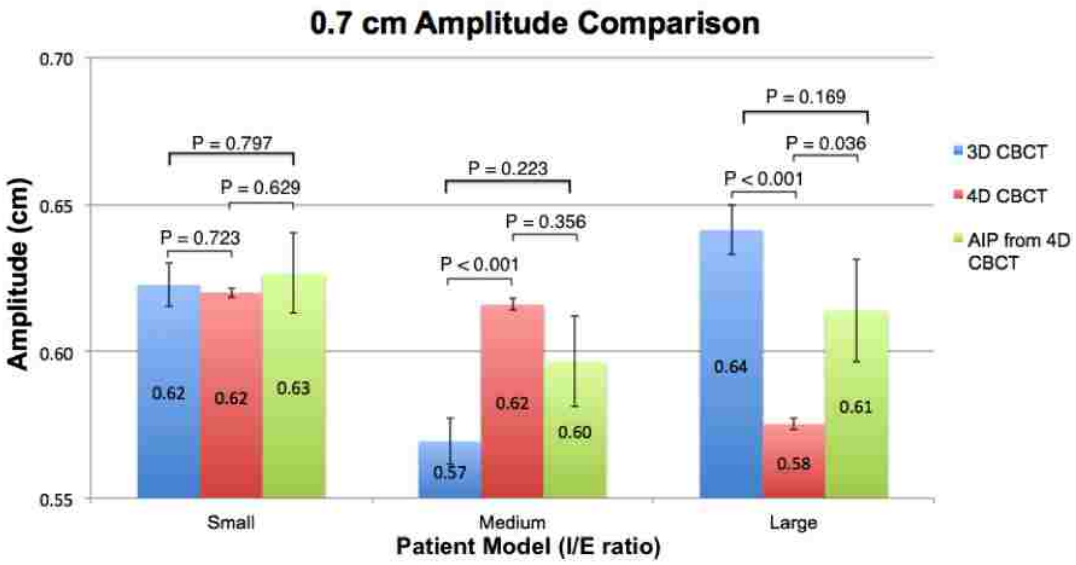

Figure 3.1: Amplitude measurements of each 0.7 cm amplitude patient model for 3D CBCT (blue), 4D CBCT (red), and AIP from 4D CBCT (green). Alphas for the independent Students t-test are displayed above the average measurements. Error bars denote the standard error. Differences in average measurements are considered significant if P < 0.017.

For the Small I/E patient model, differences in averages across all measurements were not found to be statistically significant. For the Medium I/E patient waveforms, the 4D CBCT calculated amplitude was the closest to the true amplitude but the measurement from the AIP from 4D CBCT was not found to be statistically significant (P = 0.356). For the Large I/E ratio, the 3D CBCT measurement was the closest to the true amplitude, but the difference between it and the AIP from 4D CBCT measurement was not statistically significant (P = 0.169).

Figure 3.2 shows the comparison of the amplitude measurements of each patient model moving with amplitude of 1 cm. Underestimation in measurements over all models ranged from 0.02 – 0.14 cm. For the Small and Medium I/E patient models, the AIP from 4D CBCT measurement was statistically different from the 3D CBCT and 4D CBCT measurements (P < 0.017 for all 4 comparisons).

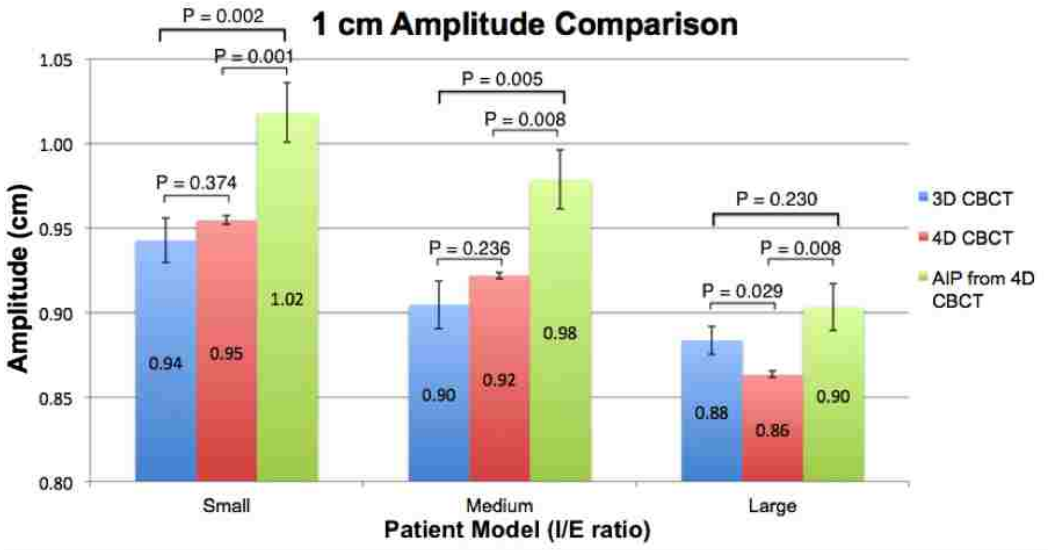

Figure 3.2: Amplitude measurements of each 1 cm amplitude patient model for 3D CBCT (blue), 4D CBCT (red), and AIP from 4D CBCT (green). Alphas for the independent Students t-test are displayed above the average measurements. Error bars denote the standard error. Differences in average measurements are considered significant if P < 0.017.

The Large I/E patient model is the only one that does not follow this trend, and this is because the difference between the AIP from 4D CBCT measurement and the 3D CBCT measurement is not statistically significant (P = 0.230).

Figure 3.3 shows the comparison of the amplitude measurements of each patient model moving with amplitude of 1.3 cm. Over all patient models, there were underestimations in the measured amplitudes from 0.01 – 0.16 cm. The AIP from 4D CBCT measurement had the smallest deviation across all patient models (0.01 – 0.03 cm) and was trending toward significance for only one other measurement, the 4D CBCT for the Small I/E patient model (P = 0.02).

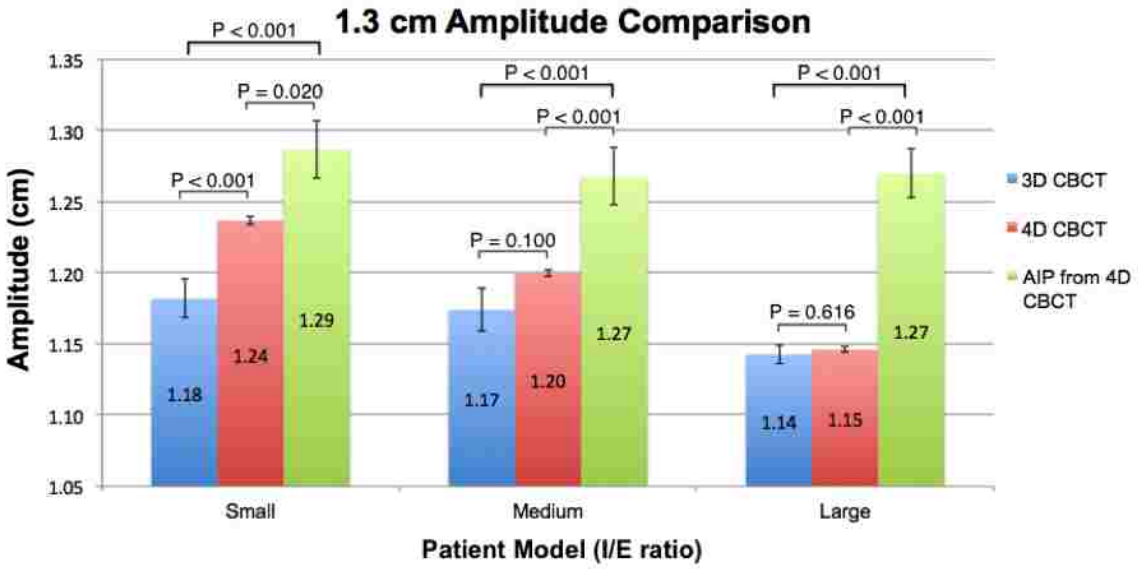

Figure 3.3: Amplitude measurements of each 1.3 cm amplitude patient model for 3D CBCT (blue), 4D CBCT (red), and AIP from 4D CBCT (green). Alphas for the independent Students t-test are displayed above the average measurements. Error bars denote the standard error. Differences in average measurements are considered significant if P < 0.017.

Figure 3.4 shows the comparison of the amplitude measurements of each patient model moving with amplitude of 1.4 cm. The averages across all measurements and patient models were underestimated from 0.02 – 0.23 cm. For the Large and Medium I/E patient models, the differences between the AIP from 4D CBCT and the 3D and 4D CBCT were statistically significant ($P < 0.001$ for all comparisons). For the Small I/E patient model, no differences between any of the measurements were significant ($P \geq 0.017$).

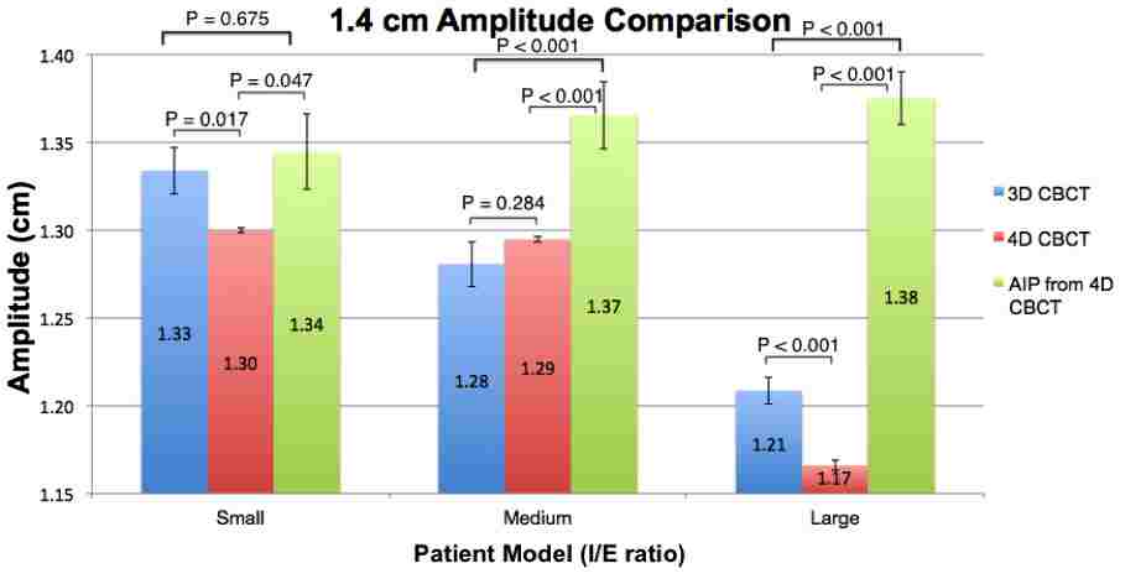

Figure 3.4: Amplitude measurements of each 1.4 cm amplitude patient model for 3D CBCT (blue), 4D CBCT (red), and AIP from 4D CBCT (green). Alphas for the independent Students t-test are displayed above the average measurements. Error bars denote the standard error. Differences in average measurements are considered significant if $P < 0.017$.

Figure 3.5 shows the comparison of the amplitude measurements of each patient model moving with amplitude of 2 cm. Averages across all measurements underestimated the amplitude of motion from 0.04 – 0.28 cm. The AIP from 4D CBCT had the smallest discrepancy in the measured amplitude across all patient models between 0.04 – 0.12 cm. The differences between

the measurement of the AIP from 4D CBCT and the 3D CBCT and 4D CBCT measurements were statistically significant for all patient models ($P < 0.001$ for all comparisons).

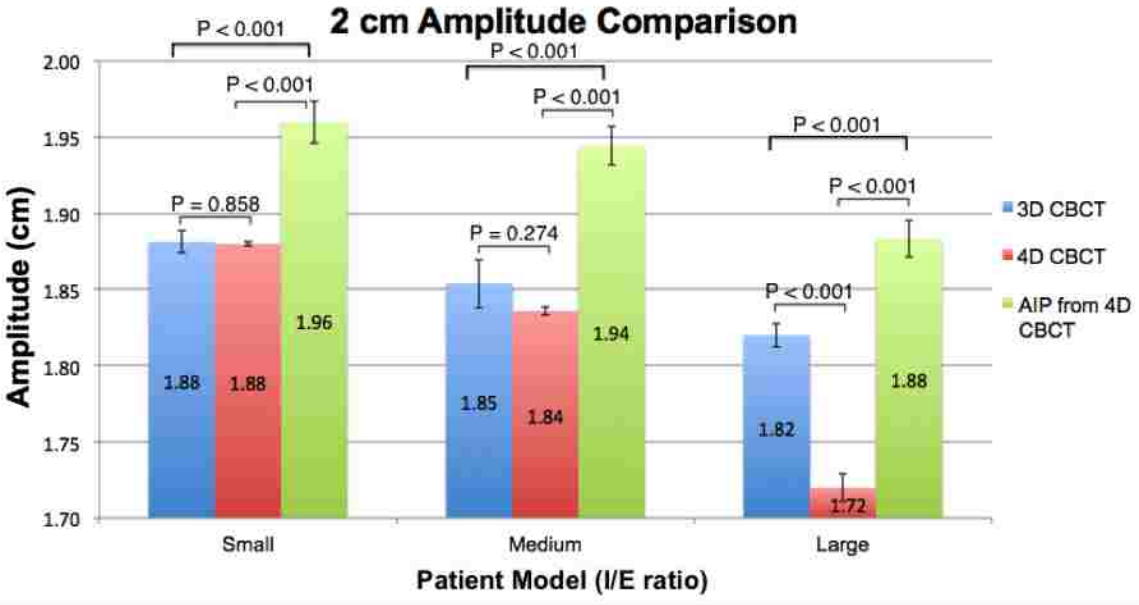

Figure 3.5: Amplitude measurements of each 2 cm amplitude patient model for 3D CBCT (blue), 4D CBCT (red), and AIP from 4D CBCT (green). Alphas for the independent Students t-test are displayed above the average measurements. Error bars denote the standard error. Differences in average measurements are considered significant if $P < 0.017$.

Figure 3.6 shows the comparison of the amplitude measurements of each patient model moving with amplitude of 2.6 cm. All differences between all average measurements for all patient models were statistically significant ($P < 0.017$). Errors in amplitude measurement ranged from 0.08 – 0.31 cm. The AIP from 4D CBCT had the smallest deviation in the measured amplitude across all patient models ranging 0.08 – 0.11 cm.

Figures 3.1 – 3.6 overwhelmingly showed that the AIP method for measurement of the motion amplitude yielded the best approximation of the motion amplitude across multiple types

of possible patient breathing. This result was more evident when the motion amplitude increased from 0.7 cm to 2.6 cm.

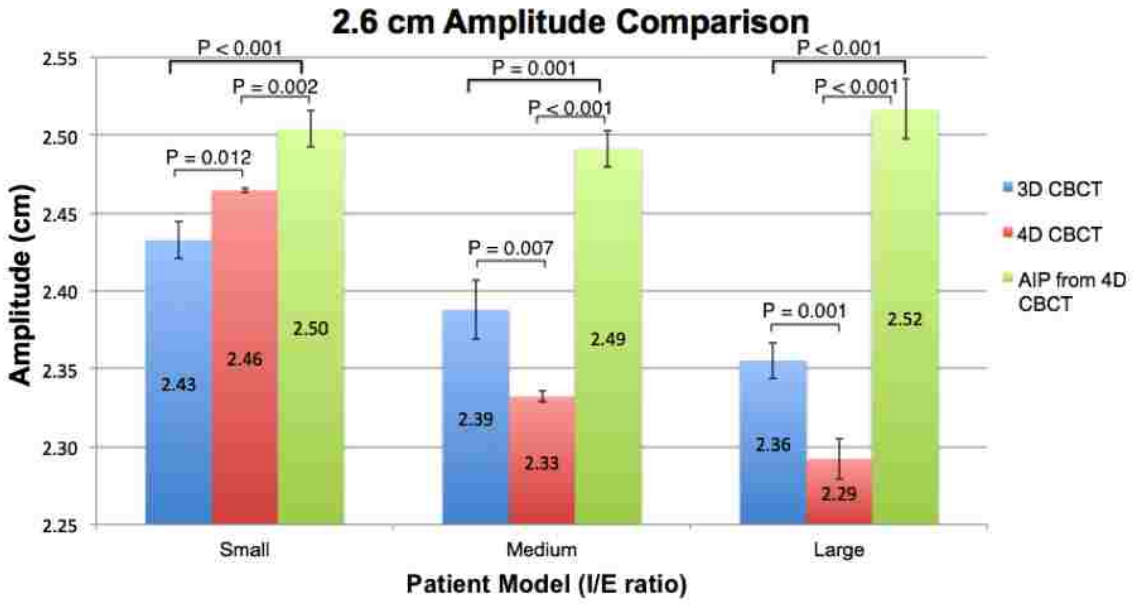

Figure 3.6: Amplitude measurements of each 2.6 cm amplitude patient model for 3D CBCT (blue), 4D CBCT (red), and AIP from 4D CBCT (green). Alphas for the independent Students t-test are displayed above the average measurements. Error bars denote the standard error. Differences in average measurements are considered significant if $P < 0.017$.

3.1.2 AMPLITUDE MEASUREMENT DISCUSSION

Overall, amplitudes measured by all localization systems were underestimated. Only one patient model measured by one system contained the true value of motion amplitude (1 cm Small I/E patient model measured by AIP from 4D CBCT, overestimation of 1.02±0.02 cm). Amplitude measured from the AIP from 4D CBCT had the smallest error when we consider all amplitudes and patient models. This result was not in line with the hypothesis that the use of 4D CBCT allows a user to measure the amplitude of tumor motion closer to reality than 3D CBCT.

The AIP from 4D CBCT measurement likely was the most accurate because the extent of tumor motion was more visually apparent and artifacts were reduced. The differences between image quality can be observed in the side-to-side comparison of a 3D CBCT image and an AIP from 4D CBCT image in Figure 3.7. Streak artifacts in the 4D CBCT phases due to view aliasing (Sonke 2005) (i.e. the lack of necessary 2D projections for reconstruction) were averaged out and the edges for user measurement were more easily found. The AIP from 4D CBCT effectively includes every acquired projection, because it is the average of 10 phases from 4D CBCT reconstruction, in total 1320 frames, compared to the 3D CBCT scan was 660 projections. Over sampling allows the most accurate generation of edges in the AIP from 4D CBCT.

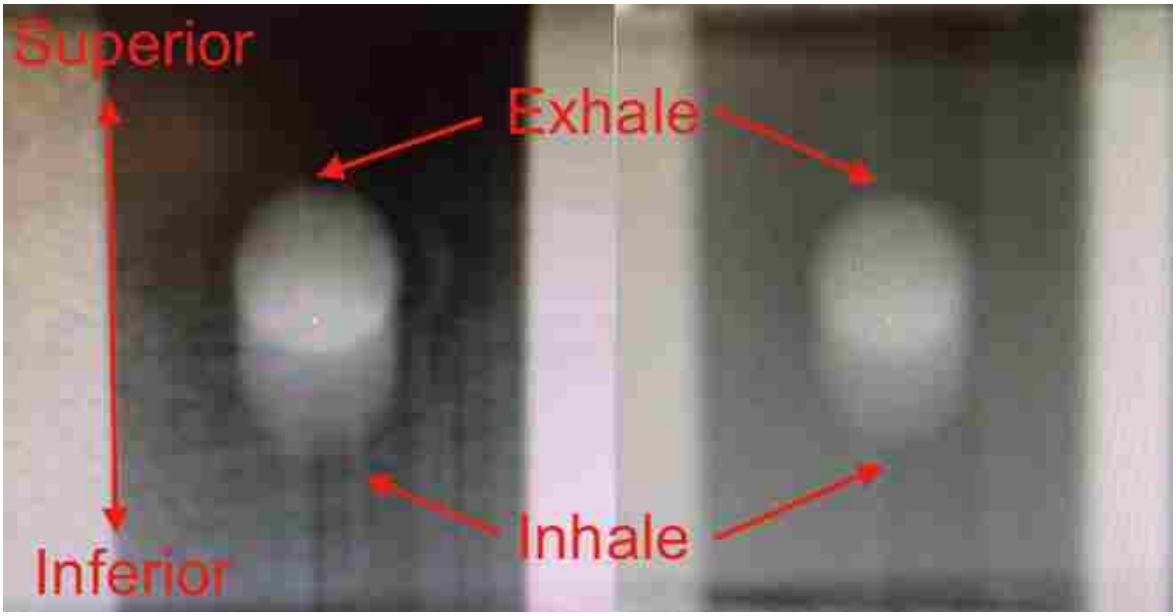

Figure 3.7: Side to side comparison of a 3D CBCT image (left) and an AIP from 4D CBCT (right).

The 4D CBCT generated amplitude was reduced compared to the other methods however, and this may seem unusual considering the performance of the AIP generated from the

4D phases. This underestimation was reported by Sonke et al. (2007), who concluded the cause was averaging within each phase bin in the 4D CBCT reconstruction (Sonke 2005).

On a patient model specific basis, we observed a general decrease in the measured amplitude as the I/E ratio increased (as less time was spent at exhale and inhale). This decrease was contrary to the study previously performed by Vergalasova et al. (Vergalasova 2011) where they examined profiles along the direction of motion. They noted that the lengths were reduced when a patient spent more time at expiration than inspiration because of contrast reduction in the SI direction, particularly at the inferior edge (corresponding to peak inhale). The reason for the opposite result in our study lies was method of measuring the edges of the target blur.

Vergalasova et al. used an edge detecting algorithm to arbitrarily determine contours, where as this study had a user measure the distance between the edges of the blur, as would be performed in a clinical workflow. Our measurements focused on the user determined mid-value between the expected CT numbers of cedar and the plastic sphere instead of software arbitrarily focused on the highest pixel values of the center of the acrylic sphere and the pixel values of the cedar. Because of this difference in techniques for measurement, the overall measurement of the amplitudes decreased from the Small I/E ratio model to the Large I/E model. This can be explained by viewing 3D CBCT images of the Small I/E and Large I/E patient models side by side in Figure 3.8.

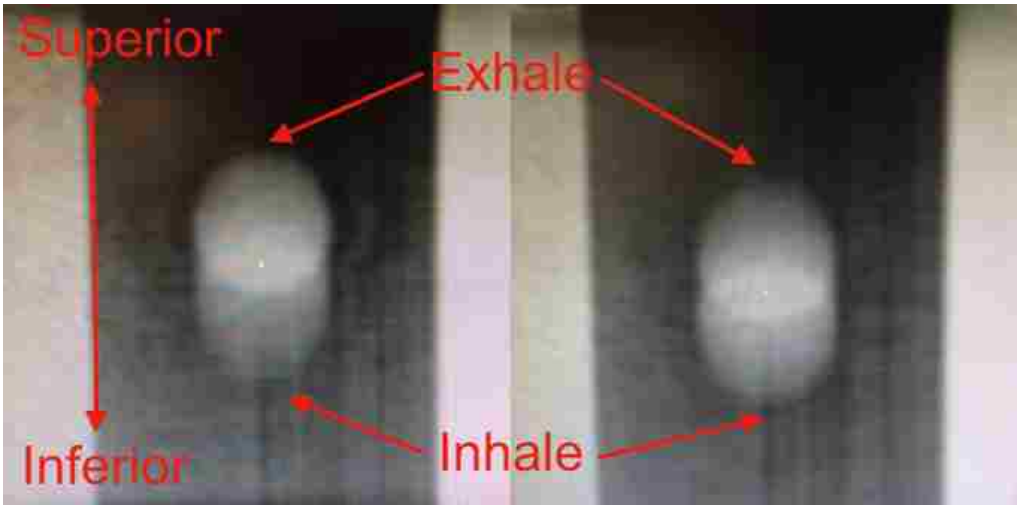

Figure 3.8: 3D CBCT images of the Small I/E patient model (left) and the Large I/E patient model (right). The Small I/E model experiences significant blurring at only one extreme (inhale, bottom) and the Large I/E model experiences significant blurring at both extremes of motion.

The superior edge (corresponding to peak exhale) was clearer for the Small I/E patient model and the inferior edge experienced more blurring. The Large I/E patient model experienced the similar blurring at both extremes of motion (exhale and inhale). In the measurement of the Large, and to a lesser extent Medium, I/E waveforms both superior and inferior edges were equally blurred due to the sharper change in position that the waveforms were chosen for. This increase in the rate of change makes the both superior and inferior edges more blurred, therefore more difficult for a user to measure.

3.1.3 SPHERE MEASUREMENT RESULTS

Figure. 3.9 shows the averages of the measurements for the tumor diameters in the exhale phases of the 4D CBCT scans. Absolute differences were less than 0.3 ± 0.9 mm in all regular patient models across the 1 cm and 2 cm amplitudes, with a 1.4 ± 1.0 mm error reported in the

irregular case (2 cm amplitude of motion only). For all regular I/E model measurements, error bars overlapped the true value of tumor diameter.

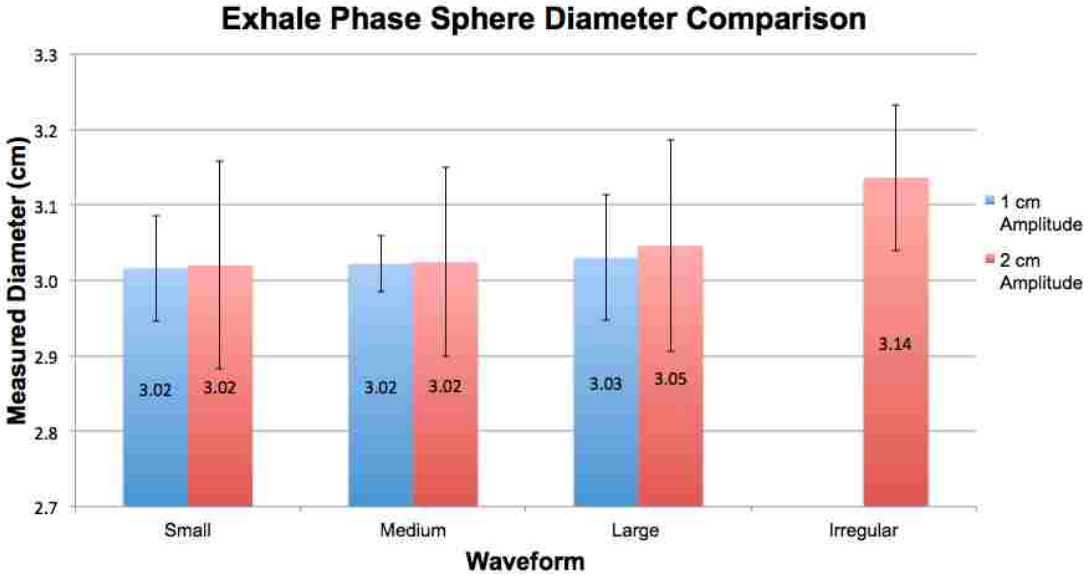

Figure 3.9: Average exhale phase sphere measurement in the SI direction for multiple motion amplitudes and patient models. Blue bars correspond to 1 cm amplitude motion during imaging and red bars corresponding to 2 cm amplitude motion during imaging. Error bars plotted represent the standard deviation of the measurements.

3.1.4 SPHERE MEASUREMENT DISCUSSION

The result from this aim confirmed the hypothesis that 4D CBCT allows for the measurement of a tumor at its exhale phase in agreement with reality, but only for regular respiratory motion. The irregular measurement was larger than the true value of the tumor because the algorithm that extracts the breathing signal from the 2D projections assumed a regular breathing pattern. When a patient breathes irregularly, the projections that were selected as closest to each breathing phase were distributed non-uniformly over the gantry rotation around the patient. To minimize artifacts, the projections were weighted during the 4D reconstruction by the gantry angle increment between projections to account for the irregularities (Sonke 2005).

3.2 AIM 2

The goal of this specific aim was to determine which IG method described in the methods section would yield the smallest error in localization in the ideal circumstance of a patient's respiratory amplitude remaining constant, or unchanged, throughout their treatment (i.e. unchanged compared to when their reference images were created). First we will review the results of the investigation into the reproducibility of the phantom set-up. Then we will review the results from the aim and discuss the findings.

3.2.1 REPRODUCIBILITY

Table 3.1 summarizes the average setup errors for all 5 phantom positions. Alignment errors were less than 0.1 mm, which is the smallest adjustment the CBCT localization software reports. As a whole across all positions, the error was 0.055 ± 0.060 mm.

Table 3.1: Average errors in phantom alignment for each position and all positions combined.

Phantom Position	Average Error in Set-up
Isocenter	0.059 ± 0.064 mm
2 mm Superior	0.054 ± 0.051 mm
5 mm Superior	0.035 ± 0.049 mm
3 mm Inferior	0.045 ± 0.051 mm
6 mm Inferior	0.065 ± 0.059 mm
All positions combined	0.055 ± 0.060 mm

These results showed that the CBCT system corrected appropriately for misalignment (within the range studied) independent of the amount of misalignment, when using the static 3D helical CT and 3D CBCT scans. Although these scans were static instead of dynamic, they confirmed the alignment of the phantom to all 5 positions was as accurate as could be achieved.

3.2.2 RESULTS

Figures in this section show average localization error for the image guidance methods used in this study (N = 90), for the regular patient respiratory models. Error bars represent the standard error of the mean. The y-axis for each plot displays the error in localization in millimeters. The statistical relationships between values are displayed as letters above or on top of the bars corresponding to the error in localization. If two columns share the same letter, then they are statistically similar ($p > 0.05$). Columns may have more than one letter above them, meaning they can be statistically significant to more than one column.

From Figure 3.10, the automatic registration of the exhale frame from 4D CBCT to the exhale frame from 4D CT was the most accurate method across all patient models, amplitudes, and offsets. The automatic exhale method had a localization error of 0.54 ± 0.03 mm, which was statistically different from all other methods.

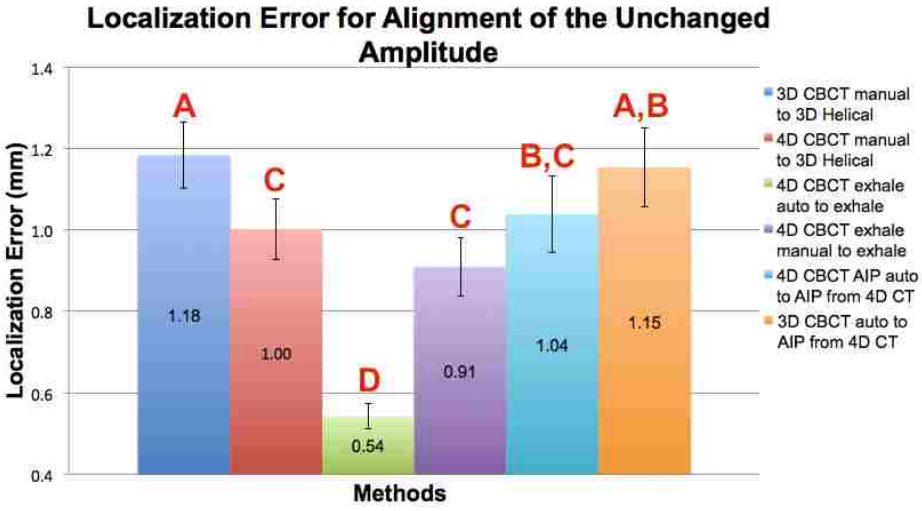

Figure 3.10: Localization Errors for image guidance methods when patient model amplitudes remains unchanged between treatment planning and CBCT localization. Error bars represent the standard error. Statistical relationships are displayed above each average (columns that share the same letter are statistically similar).

Figure 3.11 shows the localization errors separately for the two amplitudes. This plot allowed for observation of trends across the combinations of the localization method and amplitude of motion. The automatic registration of the exhale frames showed the best localization across all patient models and amplitudes of motion, although the automatic registration of the AIP from 4D CBCT to the AIP from simulation for the 1 cm amplitude patient model was statistically similar also. All methods had statistically larger errors in registration for the 2 cm amplitude except for the manual and automatic registration of exhale frames.

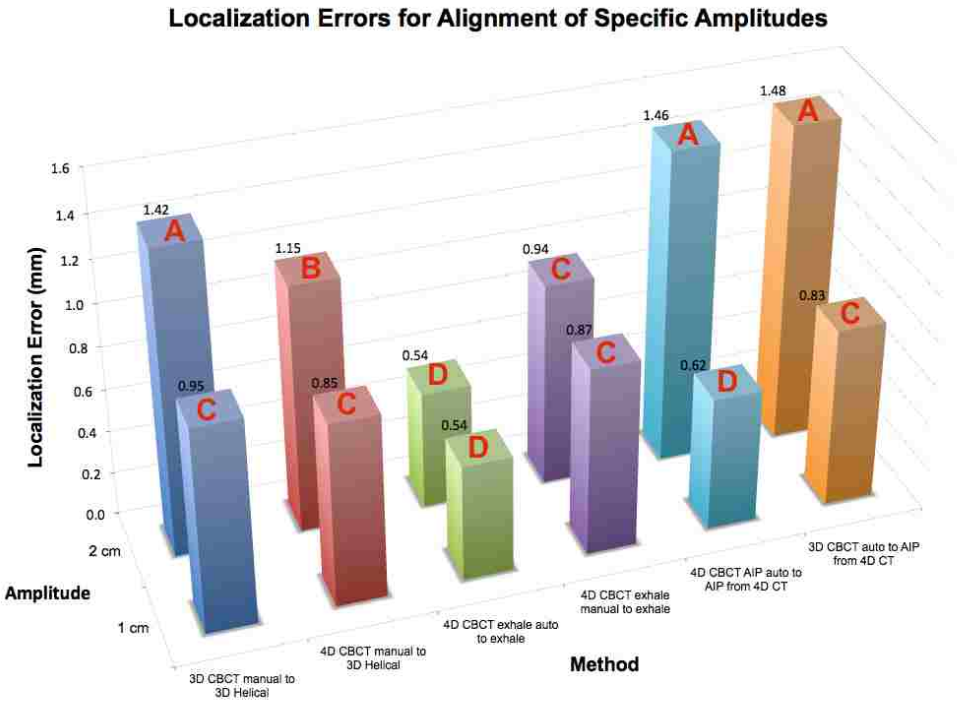

Figure 3.11: Localization Errors for combinations of image guidance methods and motion amplitudes when patient model amplitude remains unchanged between treatment planning and CBCT localization. Statistical relationships are displayed above each average (columns that share the same letter are statistically similar).

Figure 3.12 shows the localization errors separately for the three patient models. The auto exhale frame registration (green bars) had the smallest error across all patient models. The

Medium I/E patient model had errors in localization for the manual exhale registration (purple), and the two AIP reference image methods (light blue for 4D CBCT and orange for 3D CBCT) that were statistically similar to the auto exhale method (green). The smallest error in localization was observed for the Small I/E model was statistically independent from all other measurements. The pause at exhale that was represented by the Small I/E model was the most representative of patients.

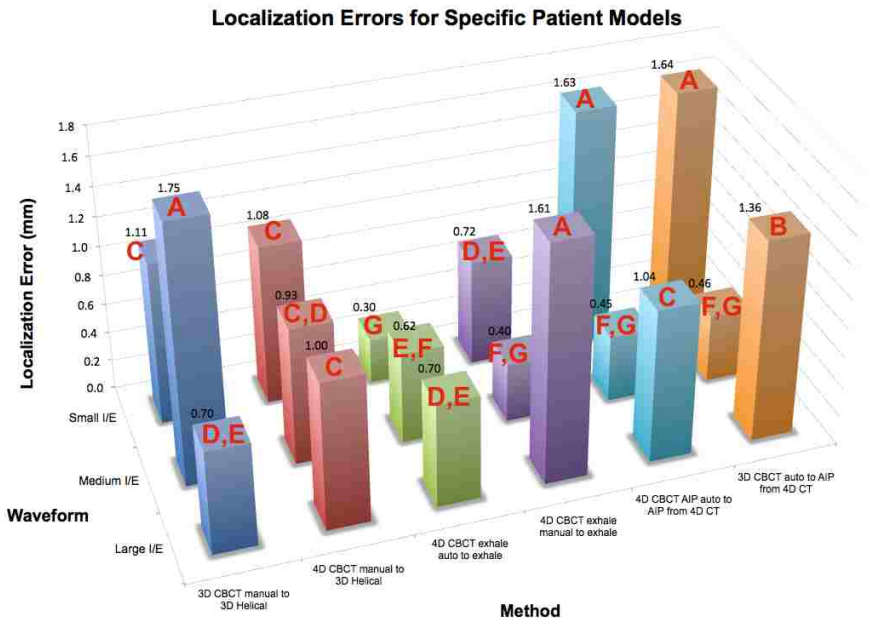

Figure 3.12: Localization Errors for combinations of image guidance methods and patient models when patient model amplitude remains unchanged between treatment planning and CBCT localization. Statistical relationships are displayed above each average (columns that share the same letter are statistically similar).

3.2.3 DISCUSSION

The results from this aim showed that the most accurate registration achievable can be provided by the use of an exhale phase from 4D CBCT localization automatically registered to a

reference exhale phase from 4D CT. The automatic registration of exhale frames resulted in a statistically significant average error in localization of 0.54 ± 0.032 mm. This finding confirmed the hypothesis that the use of the exhale frame from 4D CBCT registered to the exhale phase from 4D CT would provide statistically significant reduction in localization error compared to other 3D CBCT and 4D CBCT guidance methods. This result was determined across multiple patient models characterizing multiple possible extents of pause at exhale and different motion amplitudes. The automatic registration of exhale frames between 4D CBCT and 4D CT yielding the smallest error in localization was consistent with the literature (Sweeney, Seubert et al. 2012). The other techniques for target alignment exhibited errors ranging 0.91 – 1.18 mm. These errors were within the typical tolerance of 2 mm for lung SBRT.

3.3 AIM 3

3.3.1 RESULTS

The goal for this specific aim was to determine which IG method from Aim 2 yielded the smallest error in localization over all waveforms and amplitudes when there were changes in respiratory motion behavior between simulation and CBCT localization. The changes in behavior that were described in the methods section for Aim 3 were both an increase and a decrease of 30% in motion amplitude for all patient models. Two datasets were analyzed; each corresponding to either increased or decreased amplitude.

It must be noted that the localization performed manually by the radiation therapist was an alignment to the visible target in the reference image instead of a contour generated from a MIP superimposed onto the reference image. Comparison of the centers of the visible target and the center of a corresponding MIP showed no statistical difference between their locations nevertheless.

Figure 3.13 shows localization errors for IG methods when there was a 30% increase in the amplitude relative to simulation. As can be seen, the manual registration of the 4D CBCT to the 3D helical CT and the automatic registration of the AIP from 4D CBCT to the AIP from 4D CT showed the smallest errors (1.58 ± 0.09 mm and 1.59 ± 0.12 mm, respectively) and were statistically equivalent. The two largest average errors were observed for the exhale methods. The automatic exhale method reported 2.00 ± 0.09 mm and the manual exhale method reported 2.59 ± 0.10 mm. The localization error for the automatic registration of the 3D CBCT to the AIP from 4D CT also showed this method performed poorly, with an average error of 1.97 ± 0.12 mm, which was statistically similar to the automatic registration of exhale phases.

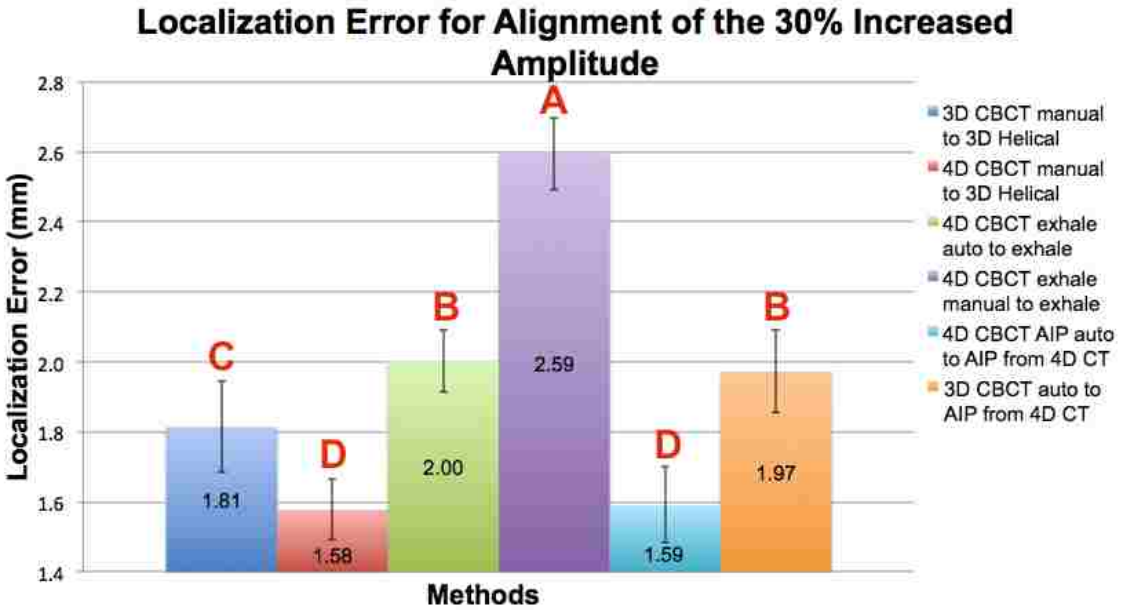

Figure 3.13: Localization Errors for image guidance methods when patient model amplitudes increase by 30% between treatment planning and CBCT localization. Error bars represent the standard error. Statistical relationships are displayed above each average (columns that share the same letter are statistically similar).

Figure 3.14 shows the localization errors for the image guidance methods when the amplitude of the sphere was decreased 30% relative to the reference image. In this case, automatic registration of the AIP from 4D CBCT automatically registered to the AIP from 4D CT had the smallest error in localization and this value was statistically different from all others, at 0.69 ± 0.02 mm. Again, the two methods utilizing the exhale frame from 4D CBCT registered to the exhale frame from 4D CT as reference yielded the largest errors in localization of 1.85 ± 0.05 mm for automatic registration and 1.26 ± 0.05 mm for the manual.

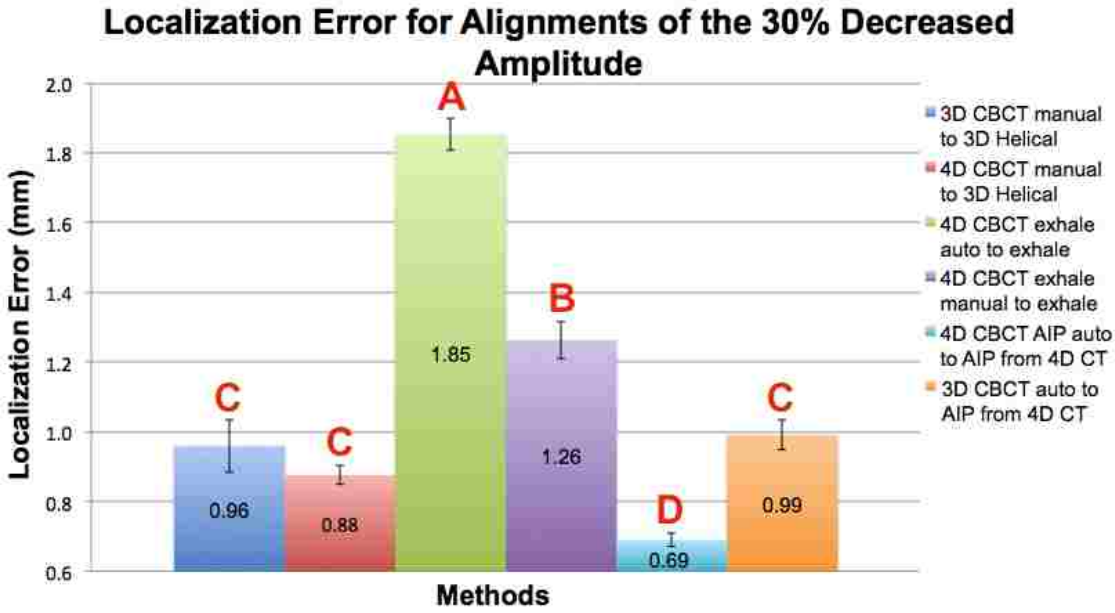

Figure 3.14: Localization Errors for image guidance methods when patient model amplitudes decrease by 30% between treatment planning and CBCT localization. Error bars represent the standard error. Statistical relationships are displayed above each average (columns that share the same letter are statistically similar).

Figure 3.15 shows the localization errors separately for the two amplitudes at reference when the amplitude of the sphere was increased by 30% during localization. For the 1 cm patient models, the AIP from 4D CBCT automatically registered to the AIP from 4D CT showed the smallest error in localization of 0.74 ± 0.05 mm, and this value was statistically different from all others. For the 2 cm patient models, the manual registration of the 4D CBCT to the 3D helical

CT had the smallest error in localization of 1.87 ± 0.08 mm. Every localization error for each method was larger for the 2 cm patient models, and all of these differences were statistically significant.

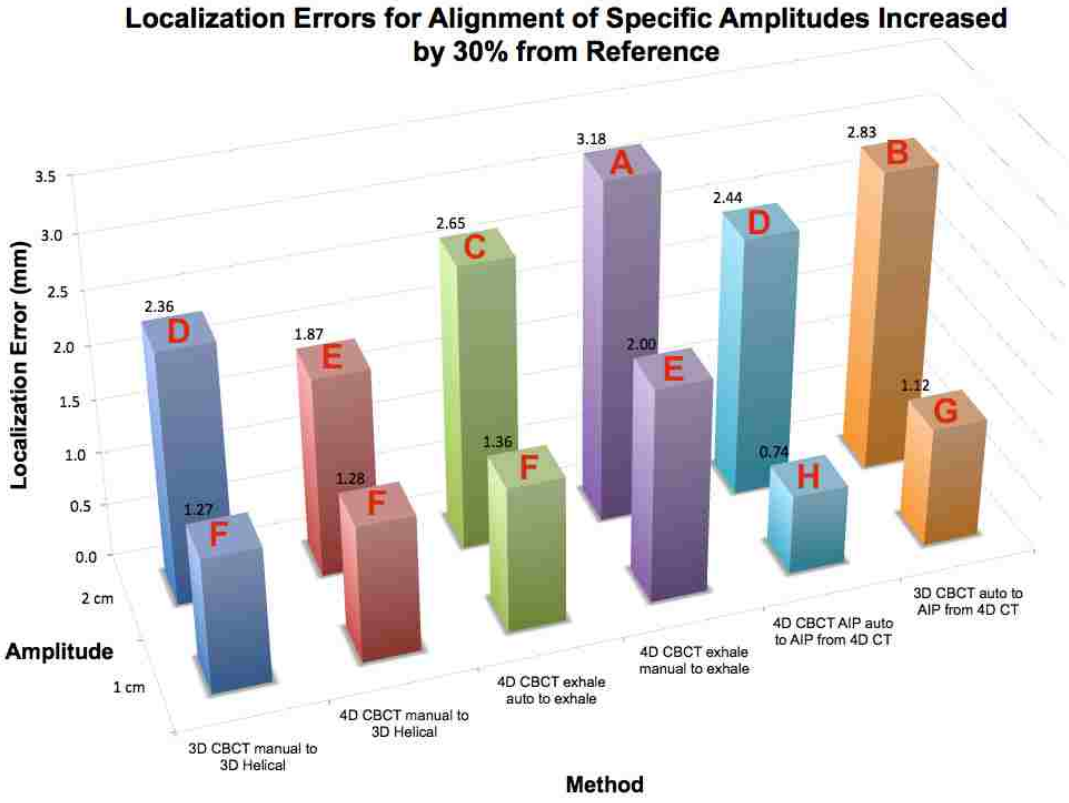

Figure 3.15: Localization Errors for combinations of image guidance methods and motion amplitudes when patient model amplitudes increased by 30% between treatment planning and CBCT localization. Statistical relationships are displayed above each average (columns that share the same letter are statistically similar).

Figure 3.16 shows the localization errors separately for the two amplitudes at reference when decreased by 30% during localization. The AIP from 4D CBCT automatically registered to the AIP from 4D CT had the smallest error of 0.50 ± 0.07 mm for the 1 cm patient models. This was statistically different to its error for the 2 cm patient models of 0.88 ± 0.08 mm The largest

error was determined for the automatic registration of the exhale phases at 2.61 ± 0.09 mm. Overall, the larger errors were experienced by methods that used the exhale phase as a reference and localization image.

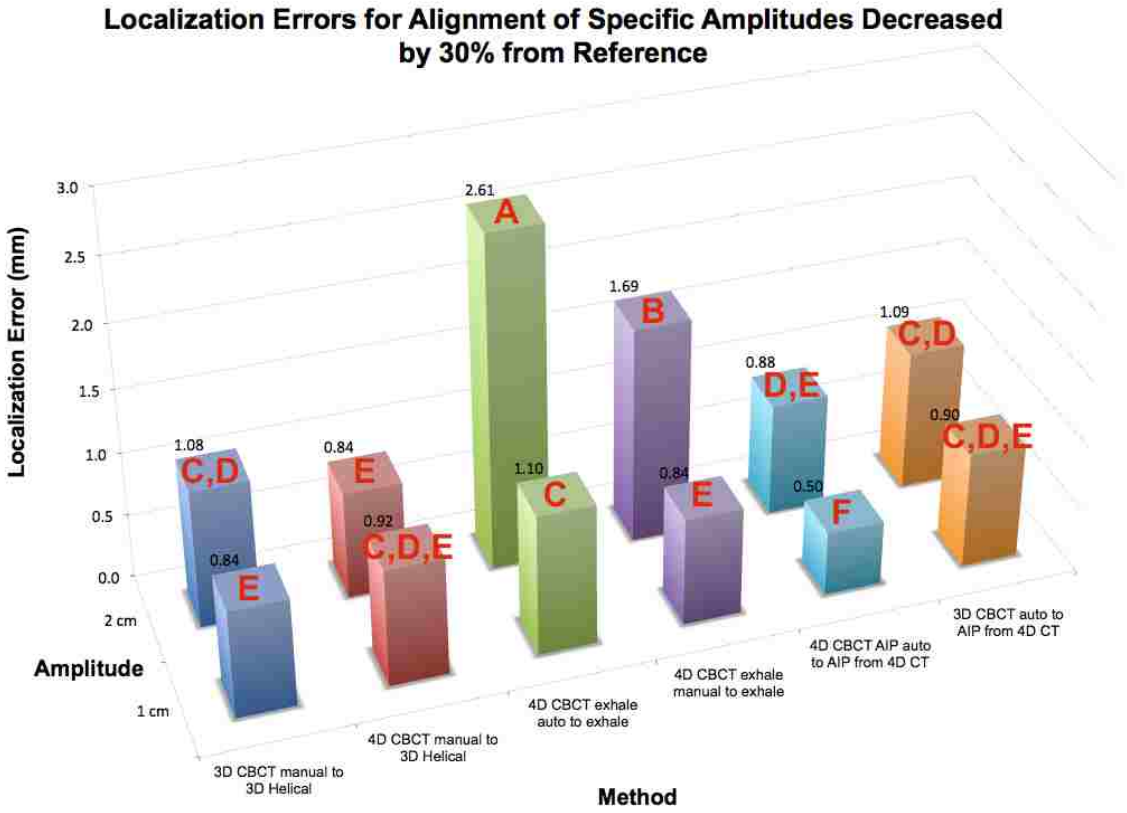

Figure 3.16: Localization Errors for combinations of image guidance methods and motion amplitudes when patient model amplitudes decrease by 30% between treatment planning and CBCT localization. Statistical relationships are displayed above each average (columns that share the same letter are statistically similar).

Figure 3.17 shows the localization errors for all image guidance methods separately for the patient models when the amplitude increased by 30% during localization. The smallest errors in localization were measured from the Large I/E patient model with 3D CBCT manually registered to a 3D helical CT (0.84 ± 0.06 mm) and the Medium I/E model with the AIP from 4D

CBCT automatically registered to the AIP from 4D CT (0.96 ± 0.06 mm), which were statistically similar. Considered independently, the Small I/E patient model had a higher average error in localization of 2.66 ± 0.03 mm across all methods which was statistically different compared to the Medium and Large I/E patient models averaging 1.46 ± 0.03 mm and 1.66 ± 0.03 mm across all methods, respectively.

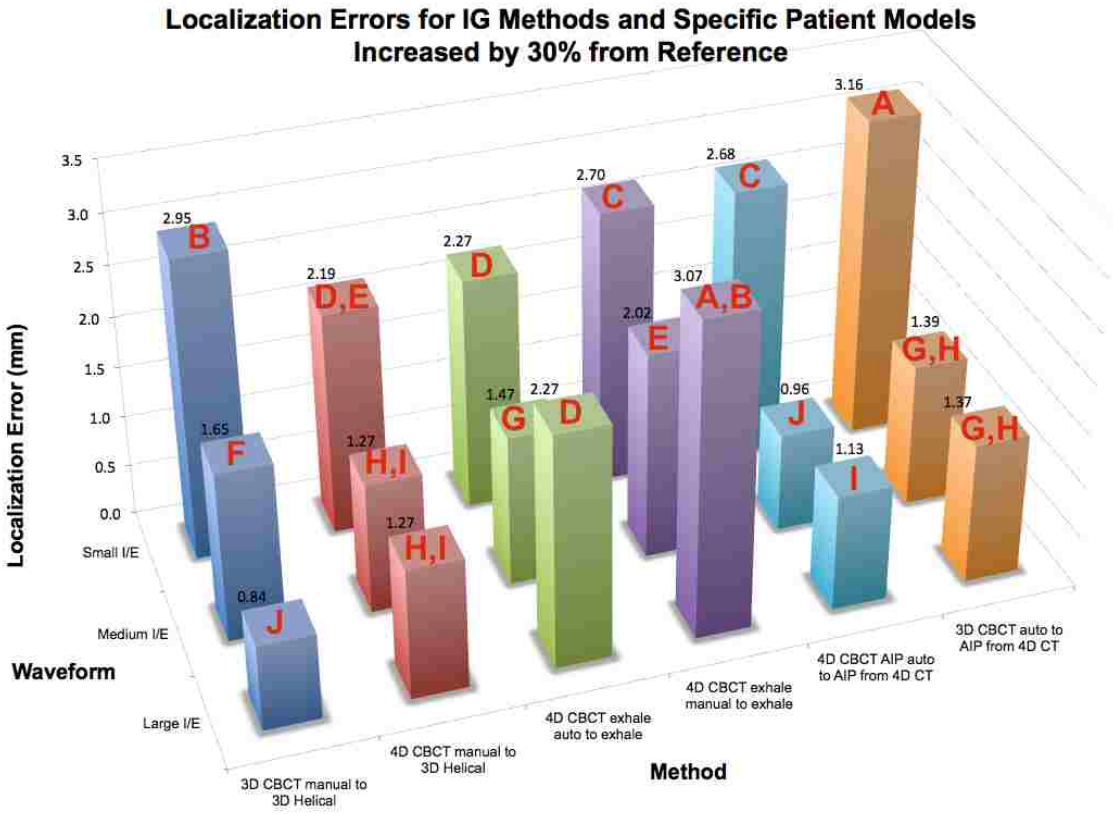

Figure 3.17: Localization Errors for combinations of image guidance methods and patient models when patient model amplitudes increase by 30% between treatment planning and CBCT localization. Statistical relationships are displayed above each average (columns that share the same letter are statistically similar).

Figure 3.18 shows the errors in localization for combinations of IG methods and patient models when the amplitude of the sphere was decreased 30% relative to the reference image.

Here the result from Figure 3.14 is clearly seen across all patient models, the automatic registration of the AIP from 4D CBCT to the 3D AIP from simulation had the smallest error. The largest error in localization was performed by the automatic registration of the exhale from 4D CBCT to the exhale from 4D CT for the Medium I/E patient model, at 2.19 ± 0.04 mm.

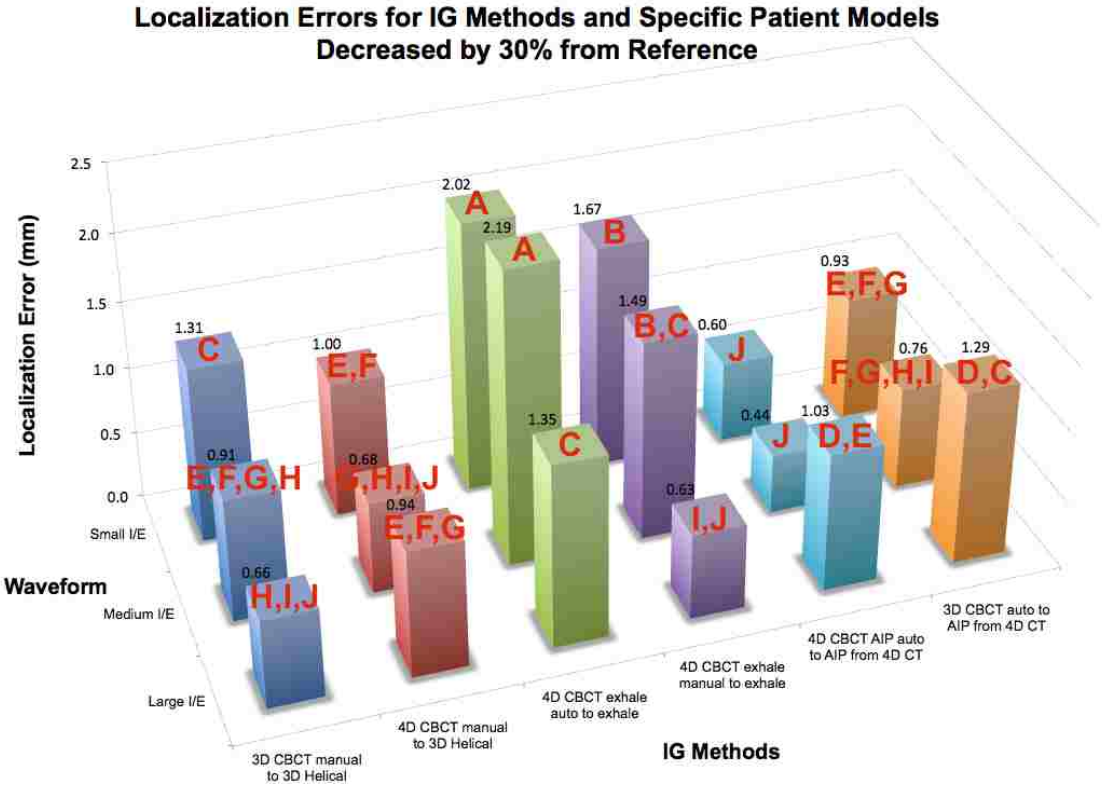

Figure 3.18: Localization Errors for combinations of image guidance methods and patient models when patient model amplitudes decrease by 30% between treatment planning and CBCT localization. Statistical relationships are displayed above each average (columns that share the same letter are statistically similar).

In summary, to simulate possible patient respiratory motion changes, the motion amplitude was increased and decreased by 30% from reference imaging for localization. The smallest error in localization when the amplitude increased by 30% from reference was achieved

by the manual registration of the 4D CBCT to the 3D helical CT (1.58 ± 0.09 mm) and the automatic registration of the AIP from 4D CBCT to the AIP from 4D CT (1.59 ± 0.12 mm); the differences were not statistically significant. The smallest error in localization when the amplitude decreased by 30% from reference was achieved through automatic registration of the AIP from 4D CBCT to the AIP from 4D CT at 0.69 ± 0.02 mm.

3.3.2 DISCUSSION

The data from this specific aim showed that the three methods for image guidance that used 4D CBCT for localization provided statistically smaller errors in localization in instances of 30% increased and decreased patient model amplitudes. This finding confirmed the hypothesis that 4D CBCT would provide a reduction in localization error compared to 3D CBCT when patient respiratory motion amplitude changed with respect to 4D CT planning. Automatic registration of the AIP from 4D CBCT to the AIP from 4D CT consistently had the smallest error in localization across both the increased and decreased motion amplitudes.

These results lead to multiple considerations when using 3D and 4D CBCT for lung SBRT. These included the most and least sensitive image guidance methods to changes in respiratory behavior and the adverse effect an increase in amplitude can have on localization motion patterns longer pause at exhale than inhale.

The most sensitive methods of image guidance to changes in respiratory motion were those that utilized an exhale phase image throughout. In Figures 3.13 and 3.14 the errors for the automatic and manual registrations of the exhale frames were the largest of all methods. When the amplitude was increased or decreased, the maximum extents of motion were changing, which were the exhale and inhale positions. When the software or user aligned them, although the

phases matched the target, the true extent of the target motion had changed, causing the motion to extend past the original range of motion, possibly outside of the field.

The least sensitive modality to changes in target motion amplitude was the AIP from 4D CBCT registered to the AIP from 4D CT. This can be attributed to the number of projections that were used in the AIP from 4D CBCT generation. It was shown in multiple studies (Sykes 2009, Lu 2010, Barber 2014) that a decreased image quality had have negative effects on a grey value automatic registration algorithm's ability to accurately match two images. A major difference between the AIP from 4D CBCT and the 3D and 4D CBCT images is the number of projections used for reconstruction: 1320 for AIP from 4D CBCT and 660 for 3D CBCT, while each phase image of 4D CBCT typically had ~130 projections.

Considered independently, the 3D CBCT had better image quality than a single phase of the 4D CBCT, due to the small number of projections in a single phase. To increase these projection numbers for a single phase, the 4D CBCT already uses a very slow gantry rotation to generate an excess of projections, but these are divided into 10 phases. By comparison, the AIP from 4D CBCT has 10 times more projections; this is twice as many as for the 3D CBCT. This greatly improved the image quality and thus allowed for a marginally better image registration as made evident in the smaller localization error across all I/E models and amplitudes.

It should be noted that the errors for localization were roughly on the order of 1 mm, so these errors are accounted for already in the margins surrounding the tumor in planning. What is more important here is not only that the 4D CBCT is marginally and statistically better than 3D CBCT, but the additional benefits and utility that 4D CBCT provides while statistically more accurate.

The use of the AIP from 4D CBCT registered to the AIP from 4D CT also proved to be a more accurate method for localization when a patient breathed irregularly. The irregular patient model was analyzed separately from the regular patient models and its results are important to the discussion for Aim 3. Figures 3.19 – 3.21 show the localization errors for the Irregular model. In the comparison of localization errors, the AIP from 4D CBCT technique provided the smallest error in localization for the irregular waveform when the amplitude of motion remained constant and when it increased 30% from reference, reporting errors of 1.78 ± 0.09 mm (Figure 3.19) and 2.91 ± 0.09 mm (Figure 3.20), respectively. These values were statistically independent.

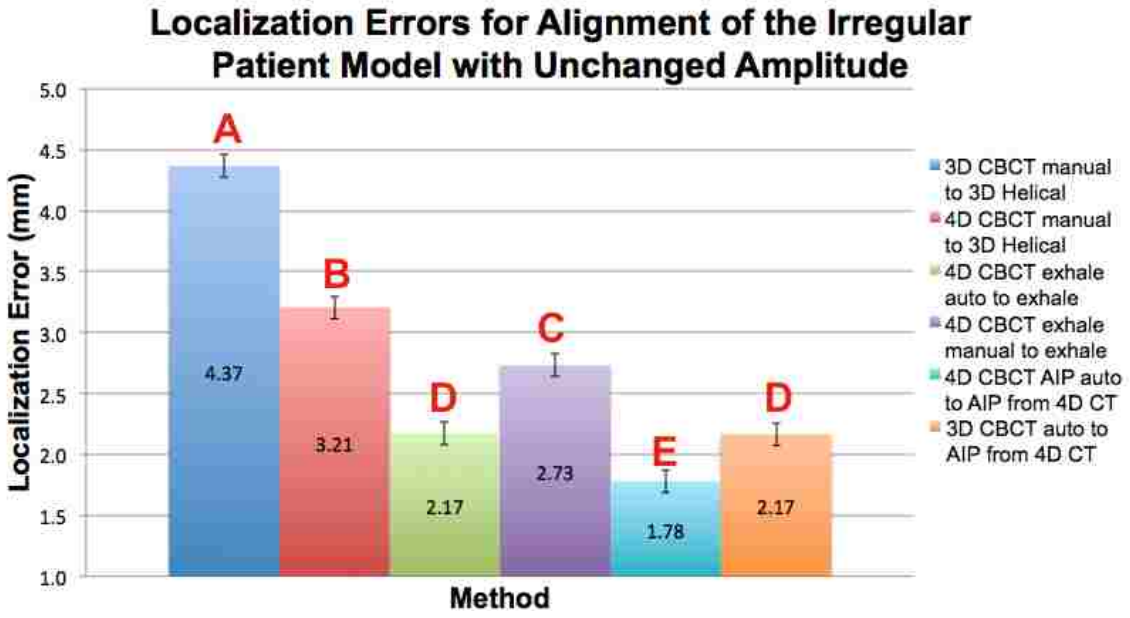

Figure 3.19: Localization errors for methods applied to the Irregular patient model unchanged from the reference image. Error bars represent the standard error of the mean. Statistical relationships are displayed above each average (columns that share the same letter are statistically similar).

For the 30% decreased amplitude from reference, the 4D CBCT AIP method had the smallest error of 0.46 ± 0.08 mm (Figure 3.21) and was statistically similar to the 4D CBCT automatic exhale method. The results from the analysis of the Irregular model localization errors further indicated the usefulness of the 4D CBCT AIP method and the lack in sensitivity to irregularities and unpredictable changes in respiratory motion amplitude.

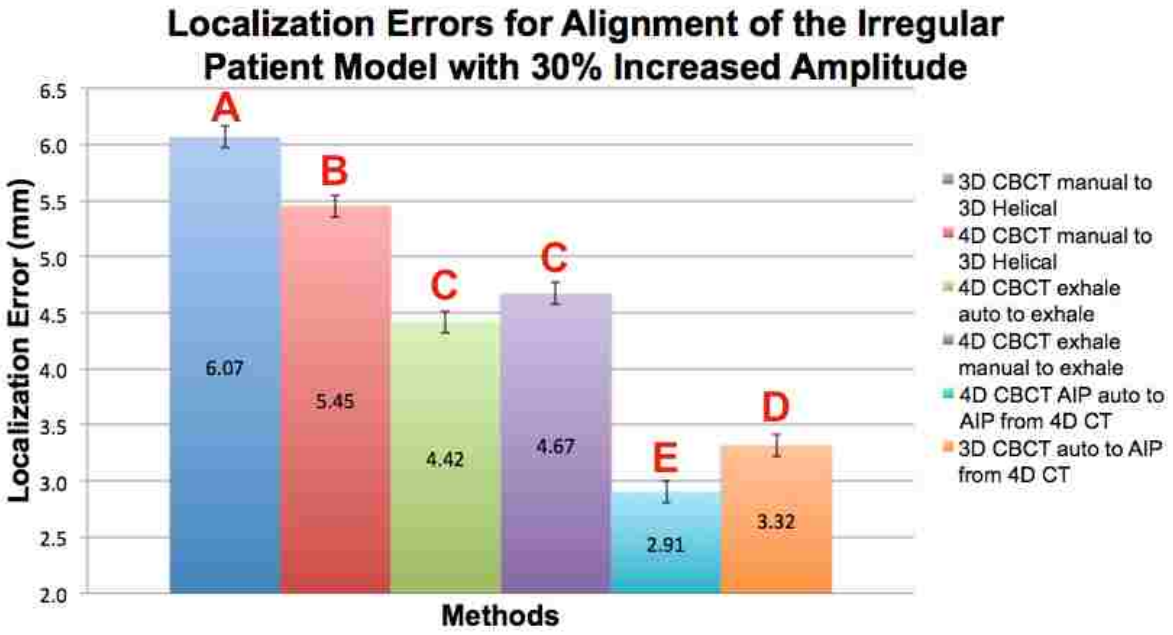

Figure 3.20: Localization errors for methods applied to the Irregular patient model increased by 30% from the reference image. Error bars represent the standard error of the mean. Statistical relationships are displayed above each average (columns that share the same letter are statistically similar).

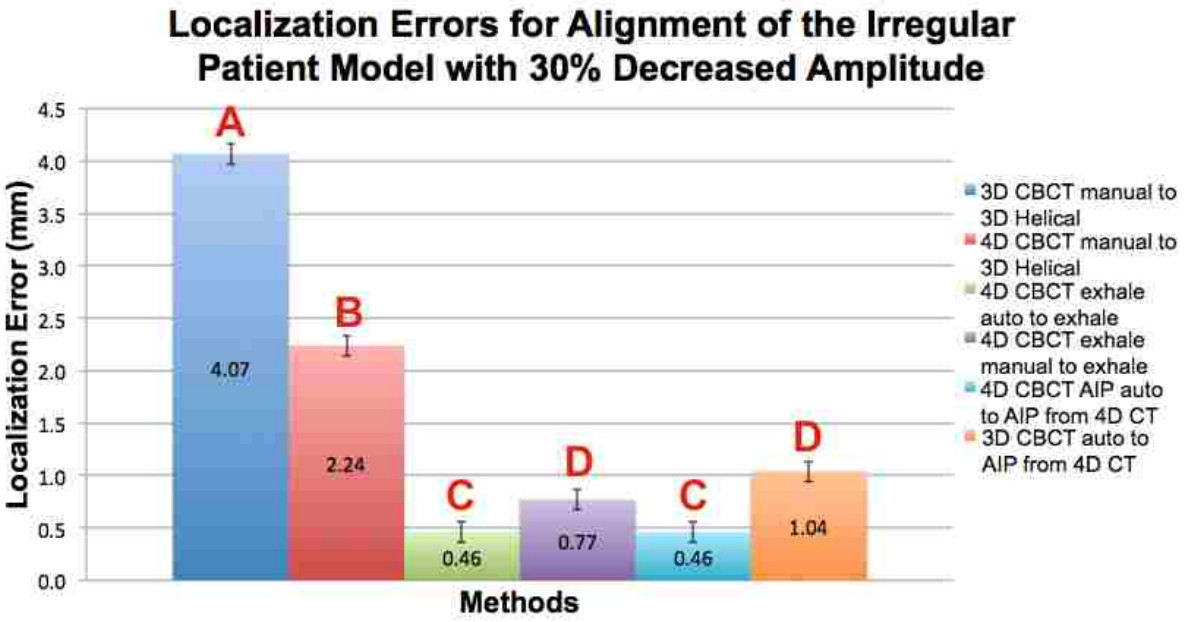

Figure 3.21: Localization errors for methods applied to the Irregular patient model decreased by 30% from the reference image. Error bars represent the standard error of the mean. Statistical relationships are displayed above each average (columns that share the same letter are statistically similar).

The second trend evident in the results from Aim 3 was the large error experienced by all 3D CBCT and 4D CBCT methods for the Small I/E ratio patient model when the amplitude increased by 30% compared to reference (Figure 3.17). The average error in localization across all methods was 2.66 ± 0.03 mm for the Small I/E model which was statistically different compared to the Medium and Large I/E models averaging 1.46 ± 0.03 mm and 1.66 ± 0.03 mm. When a target spent more than twice as much time close to peak exhale than peak inhale, a 30% increase in their respiratory amplitude caused clinically significant errors in target alignment (>2 mm). When a target spent more time at one location (i.e. exhale) more projections were generated for that position, which biased the pixel intensities toward that location. Changes in that location, especially when the time spent there was long, caused software and users to consistently align the target to the radiation field incorrectly.

As stated in the background, 4D CBCT improved target visualization (Sonke 2005, Sweeney 2012), allowed a user to verify details of a target immediately prior to treatment without motion blurring biasing the shape of the tumor (Sonke 2005), and allowed for the independent localization of specific phases of motion (Purdie 2006). All these benefits, as well as the statistical difference from the 3D CBCT method, and the overall best localization when a patient's tumor motion amplitude increased or decreased between reference and localization indicated that the use of 4D CBCT for initial viewing to assess motion change of the tumor during all phases, and then registration of the AIP generated from the 4D CBCT to an AIP created from the 4D CT will yield the most accurate target alignment with clinically available resources. This was additionally supported by the method's performance when a patient breathes irregularly throughout the image guidance process.

CHAPTER 4: CONCLUSIONS

4.1 AIM 1

For all methods of measuring the amplitude, there was a systemic underestimation, of approximately 2 mm. Across all methods, the amplitude from the 4D-CBCT AIP had the smallest error, and this can be attributed to the number of projections that went into the AIP from 4D CBCT, greatly increasing image quality and allowing for the best conditions for user measurement.

In the exhale phase of the 4D CBCT there was excellent agreement between the measurement of the sphere diameter and the reality, with averages slightly larger than the truth of roughly 0.2 mm, although it should be noted that the standard deviations contained 3 cm for all regular patient models. This indicated that 4D CBCT reconstruction is able to produce phase imagery that is representative of actual mobile target dimensions.

Aim 1 confirmed 4D CBCT's ability to generate representative imagery of a moving target. The availability of this technology allows physicians and therapists to glean more information such as the specific movement of a target in three dimensions from a process that was originally intended only to provide target alignment.

4.2 AIM 2

The automatic registration of exhale frames between 4D CT and 4D CBCT resulted in the smallest average error in localization of 0.54 ± 0.032 mm when the same target motion amplitude is used throughout image guidance. This finding confirmed the hypothesis that the use of the exhale frame from 4D CBCT registered to the exhale phase from 4D CT would provide statistically significant reduction in localization error compared to other 3D and 4D CBCT guidance methods. This result was determined across multiple patient models characterizing

multiple possible extents of pause at exhale and different motion amplitudes of 1 and 2 cm. Sub millimeter target alignments can be achieved if a patient breathes with the same amplitude throughout treatment and automatic registration of exhale frames is used for image guidance.

Aim 2 indicated that extremely accurate target alignment can be achieved with 4D CBCT exhale frame registration. The great reduction in localization error compared to other methods allows for reduced target margins usually present to account for the localization errors. A reduced margin compared to the current case will irradiate less healthy tissue and improve overall patient performance in lung SBRT (Benedict 2010).

4.3 AIM 3

Due to uncertainties pertaining to patient respiratory behavior throughout lung SBRT fractions, the use of an image guidance technique that can both recognize these changes, and accurately align despite them is extremely important. The method of obtaining an AIP from 4D CBCT for registration to a reference AIP from 4D CT accurately localized mobile targets whether or not they underwent changes in respiratory amplitude. This technique is accurate across multiple types of breathing and extents of target motion, and has the added utility and increase in target visualization that 4D CBCT allows. The method of an AIP from 4D CBCT automatically registered to a reference AIP from 4D CT should be used when treating lung SBRT cases with 4D CBCT. The reduction in workflow and slight increase in dose compared to 3D CBCT is negligible when the large amount of time required for an SBRT treatment and the high doses per fraction and fewer number of fractions are considered.

4.4 FUTURE WORK

Recently, the use of a breath hold technique during lung radiation therapy with standard fractionation (approx. 2 Gy/fraction) was implemented at Mary Bird Perkins Cancer Center in

Baton Rouge, LA. In these cases, the patient had a video monitor within their visual field that showed the movement of a reflector box on their abdomen. For the breath hold, they were asked to hold their breath at maximum inhale, aligning a point on the reflector box to a line corresponding to the maximum inhale position that was imaged during planning. This treatment technique required a greatly increased treatment time as well as time for the planning and set up of the treatment. What can be taken from this and applied to 4D CBCT is the system self-monitored patient breathing. Our study showed that the smallest errors in localization occurred when the patient breathes the same at reference as at localization; thus self-monitored patient breathing control may be potentially advantageous. Further investigation into this theory is required.

REFERENCES

Barber, J., J. R. Sykes, L. Holloway and D. I. Thwaites (2014). "Automatic image registration performance for two different CBCT systems; variation with imaging dose." Journal of Physics: Conference Series **489**: 012070.

Benedict, S. H., K. M. Yenice, D. Followill, J. M. Galvin, W. Hinson, B. Kavanagh, P. Keall, M. Lovelock, S. Meeks, L. Papiez, T. Purdie, R. Sadagopan, M. C. Schell, B. Salter, D. J. Schlesinger, A. S. Shiu, T. Solberg, D. Y. Song, V. Stieber, R. Timmerman, W. A. Tomé, D. Verellen, L. Wang and F.-F. Yin (2010). "Stereotactic body radiation therapy: The report of AAPM Task Group 101." Med Phys **37**(8): 4078.

Bissonnette, J. P., K. N. Franks, T. G. Purdie, D. J. Moseley, J. J. Sonke, D. A. Jaffray, L. A. Dawson and A. Bezjak (2009). "Quantifying interfraction and intrafraction tumor motion in lung stereotactic body radiotherapy using respiration-correlated cone beam computed tomography." Int J Radiat Oncol Biol Phys **75**(3): 688-695.

Borst, G., J. J. Sonke, A. Betgen, P. Remeijer, M. van Herk and J. Lebesque (2007). "Kilo-voltage cone-beam computed tomography setup mea- surements for lung cancer patients; first clinical results and comparison with electronic portal-imaging device." Int J Radiat Oncol Biol Phys **68**: 555-561.

Groh, B. A., J. H. Siewerdsen, D. G. Drake, J. W. Wong and D. A. Jaffray (2002). "A performance comparison of flat-panel imager-based MV and kV cone-beam CT." Med Phys **29**(6): 967.

Guckenberger, M., J. Meyer, J. Wilbert, A. Richter, K. Baier, G. Mueller and M. Flentje (2007). "Intra-fractional uncertainties in cone-beam CT based image-guided radiotherapy (IGRT) of pulmonary tumors." Radiother Oncol **83**(1): 57-64.

Guckenberger, M., J. Wilbert, T. Krieger, A. Richter, K. Baier and M. Flentje (2009). "Mid-ventilation concept for mobile pulmonary tumors: internal tumor trajectory versus selective reconstruction of four-dimensional computed tomography frames based on external breathing motion." Int J Radiat Oncol Biol Phys **74**(2): 602-609.

Hill, D. L. G., P. G. Batchelor, M. Holden and D. J. Hawkes (2001). "Medical image registration." Phys Med Biol **46**: R1-R45.

Hugo, G. D., J. Liang, J. Campbell and D. Ian (2007). "Online target position localization in the presence of respiration: a comparison of two methods." Int J Radiat Oncol Biol Phys **69**(5): 1634-1641.

ICRU (1993). "Prescribing, recording, and reporting photon beam therapy." ICRU Report 50.

Keall, P. J., G. S. Mageras, J. M. Balter, R. S. Emery, K. M. Forster, S. B. Jiang, J. M. Kapatoes, D. A. Low, M. J. Murphy, B. R. Murray, C. R. Ramsey, M. B. Van Herk, S. S. Vedam, J. W. Wong and E. Yorke (2006). "The management of respiratory motion in radiation oncology report of AAPM Task Group 76." Med Phys **33**(10): 3874.

Langner, U. W. and P. J. Keall (2010). "Quantification of artifact reduction with real-time cine four-dimensional computed tomography acquisition methods." Int J Radiat Oncol Biol Phys **76**(4): 1242-1250.

Li, T., L. Xing, P. Munro, C. McGuinness, M. Chao, Y. Yang, B. Loo and A. Koong (2006). "Four-dimensional cone-beam computed tomography using an on-board imager." Med Phys **33**(10): 3825.

Liu, H. H., P. Balter, T. Tutt, B. Choi, J. Zhang, C. Wang, M. Chi, D. Luo, T. Pan, S. Hunjan, G. Starkschall, I. Rosen, K. Prado, Z. Liao, J. Chang, R. Komaki, J. D. Cox, R. Mohan and L. Dong (2007). "Assessing respiration-induced tumor motion and internal target volume using four-dimensional computed tomography for radiotherapy of lung cancer." Int J Radiat Oncol Biol Phys **68**(2): 531-540.

Lovelock, D. M., C. Hua, P. Wang, M. Hunt, N. Fournier-Bidoz, K. Yenice, S. Toner, W. Lutz, H. Amols, M. Bilsky, Z. Fuks and Y. Yamada (2005). "Accurate setup of paraspinal patients using a noninvasive patient immobilization cradle and portal imaging." Med Phys **32**(8): 2606.

Lu, B., H. Lu and J. Palta (2010). "A comprehensive study on decreasing the kilovoltage cone-beam CT dose by reducing the projection number." J Appl Clin Med Phys **11**(3): 231-249.

Murray, B., K. Forster and R. Timmerman (2007). "Frame-based immobilization and targeting for stereotactic body radiation therapy." Med Dosim **32**(2): 86-91.

Nagata, Y., Y. Kegoro, T. Aoki, T. Mizowaki, K. Takayama, M. Kokubo, N. Araki, M. Mitsumori, K. Sasai, Y. Shibamoto, S. Koga, S. Yano and M. Hiraoka (2002). "Clinical outcomes of 3D conformal hypofractionated single high-dose radiotherapy for one or two lung tumors using a stereotactic body frame." Int J Radiat Oncol Biol Phys **52**(4): 1041-1046.

Poulsen, P. R., B. Cho and P. J. Keall (2008). "A method to estimate mean position, motion magnitude, motion correlation, and trajectory of a tumor from cone-beam CT projections for image-guided radiotherapy." Int J Radiat Oncol Biol Phys **72**(5): 1587-1596.

Purdie, T. G., J. P. Bissonnette, K. Franks, A. Bezjak, D. Payne, F. Sie, M. B. Sharpe and D. A. Jaffray (2007). "Cone-beam computed tomography for on-line image guidance of lung stereotactic radiotherapy: localization, verification, and intrafraction tumor position." Int J Radiat Oncol Biol Phys **68**(1): 243-252.

Purdie, T. G., D. J. Moseley, J. P. Bissonnette, M. B. Sharpe, K. Franks, A. Bezjak and D. A. Jaffray (2006). "Respiration correlated cone-beam computed tomography and 4DCT for evaluating target motion in Stereotactic Lung Radiation Therapy." Acta Oncol **45**(7): 915-922.

Rietzel, E., T. Pan and G. T. Y. Chen (2005). "Four-dimensional computed tomography: Image formation and clinical protocol." Med Phys **32**(4): 874.

Song, J. Y., T. K. Nam, S. J. Ahn, W. K. Chung, M. S. Yoon and B. S. Nah (2009). "Respiratory motional effect on cone-beam CT in lung radiation surgery." Med Dosim **34**(2): 117-125.

Sonke, J.-J., L. Zijp, P. Remeijer and M. van Herk (2005). "Respiratory correlated cone beam CT." Med Phys **32**(4): 1176.

Sonke, J. J., M. Rossi, J. Wolthaus, M. van Herk, E. Damen and J. Belderbos (2009). "Frameless stereotactic body radiotherapy for lung cancer using four-dimensional cone beam CT guidance." Int J Radiat Oncol Biol Phys **74**(2): 567-574.

Sweeney, R. A., B. Seubert, S. Stark, V. Homann, G. Muller, M. Flentje and M. Guckenberger (2012). "Accuracy and inter-observer variability of 3D versus 4D cone-beam CT based image-guidance in SBRT for lung tumors." Radiat Oncol **7**: 81.

Sykes, J. R., D. S. Brettle, D. R. Magee and D. I. Thwaites (2009). "Investigation of uncertainties in image registration of cone beam CT to CT on an image-guided radiotherapy system." Phys Med Biol **54**(24): 7263-7283.

Timmerman, R., B. Kavanagh, L. Cho, L. Papiez and L. Xing (2007). "Stereotactic body radiation therapy in multiple organ sites." J Clin Oncol **25**(8): 947-952.

Timmerman, R. D. (2008). "An overview of hypofractionation and introduction to this issue of seminars in radiation oncology." Semin Radiat Oncol **18**(4): 215-222.

Vergalasova, I., J. Maurer and F.-F. Yin (2011). "Potential underestimation of the internal target volume (ITV) from free-breathing CBCT." Med Phys **38**(8): 4689.

Wang, L., X. Chen, M. H. Lin, J. Xue, T. Lin, J. Fan, L. Jin and C. M. Ma (2013). "Evaluation of the cone beam CT for internal target volume localization in lung stereotactic radiotherapy in comparison with 4D MIP images." Med Phys **40**(11): 111709.

Wang, Z., Q. J. Wu, L. B. Marks, N. Larrier and F. F. Yin (2007). "Cone-beam CT localization of internal target volumes for stereotactic body radiotherapy of lung lesions." Int J Radiat Oncol Biol Phys **69**(5): 1618-1624.

Wolthaus, J. W., J. J. Sonke, M. van Herk, J. S. Belderbos, M. M. Rossi, J. V. Lebesque and E. M. Damen (2008). "Comparison of different strategies to use four-dimensional computed tomography in treatment planning for lung cancer patients." Int J Radiat Oncol Biol Phys **70**(4): 1229-1238.

Wulf, J., U. Hadinger, U. Oppitz, B. Olshausen and M. Flentje (2000). "Stereotactic radiotherapy of extracranial targets: CT-simulation and accuracy of treatment in the stereotactic body frame." Radiother Oncol **57**(2): 225-236.

Yin, F. F., J. Wong, J. Balter, S. H. Benedict, J. P. Bissonnette, T. Craig, L. Dong, D. A. Jaffray, S. Jiang, S. Kim, C. M. Ma, M. Murphy, P. Munro, T. Solberg and J. Wu (2009). "The Role of In-Room kV X-Ray Imaging for Patient Setup and Target Localization: Report of Task Group 104 of the Therapy Imaging Committee." Med Phys **70**(104).

Zijp, L., J. J. Sonke and M. Herk (2004). "Extraction of the respiratory signal from sequential thorax cone-beam X-ray images." International Conference on the Use of Computers in Radiation Therapy: 507-509.

APPENDIX A: REFERENCE IMAGES AND CONTOURS

This section displays all reference images and contours after completion in the TPS, prior to export to the CBCT system.

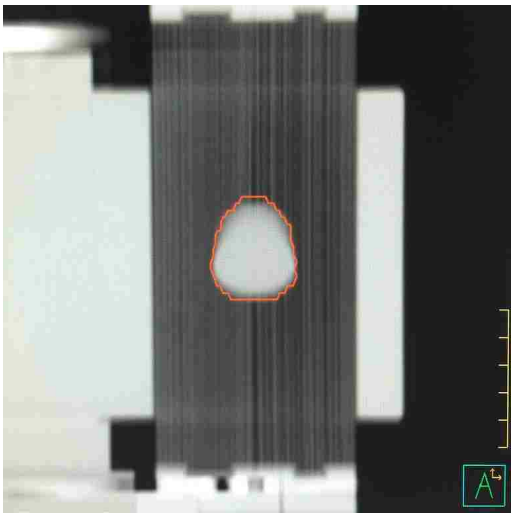

Figure A.1: 3D helical CT reference image of the 1 cm amplitude Small I/E patient model.

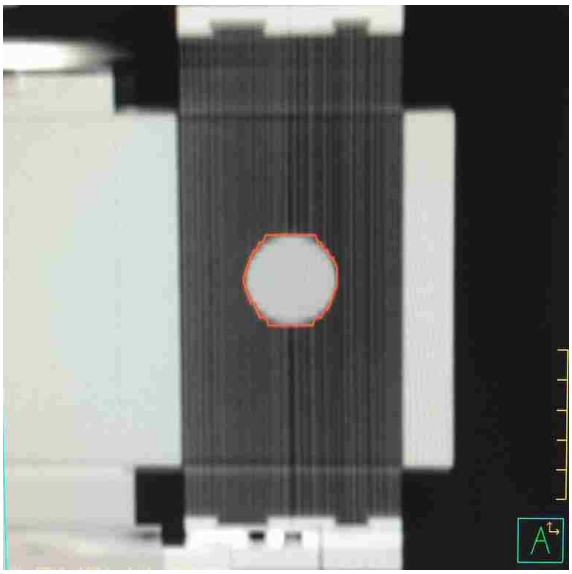

Figure A.2: Exhale from 4D CT reference image of the 1 cm Small I/E patient model.

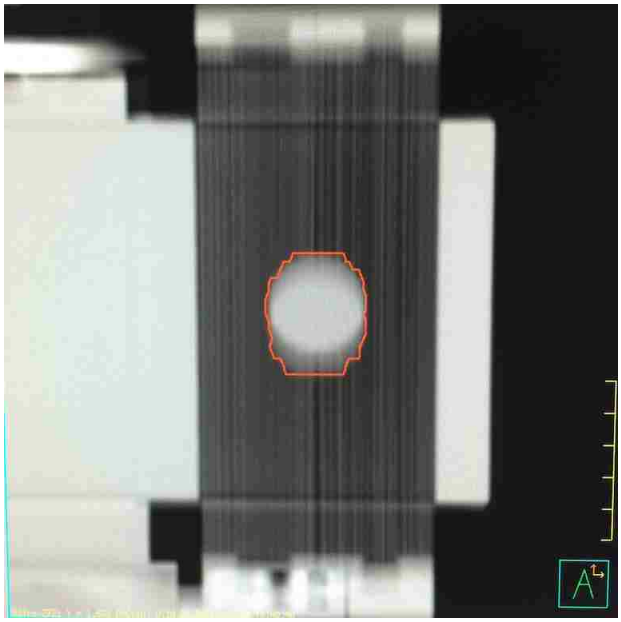

Figure A.3: AIP from 4D CT reference image of the 1 cm Small I/E patient model.

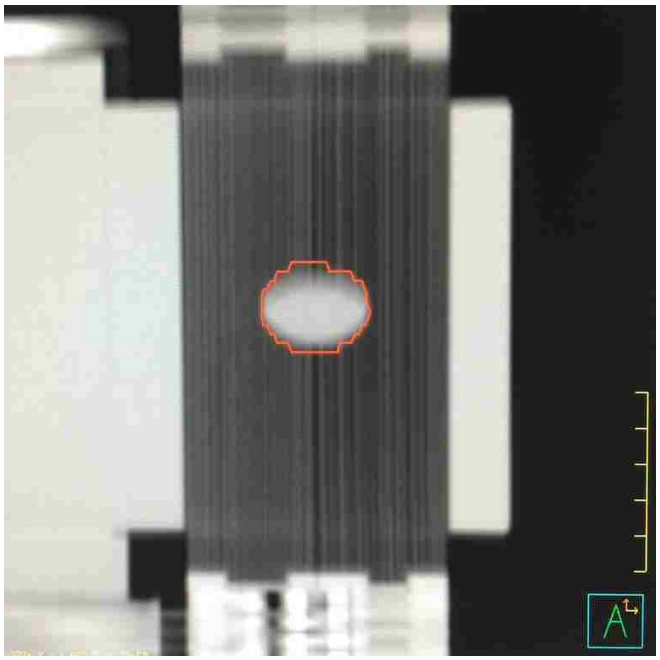

Figure A.4: 3D helical CT reference image of the 2 cm Small I/E patient model.

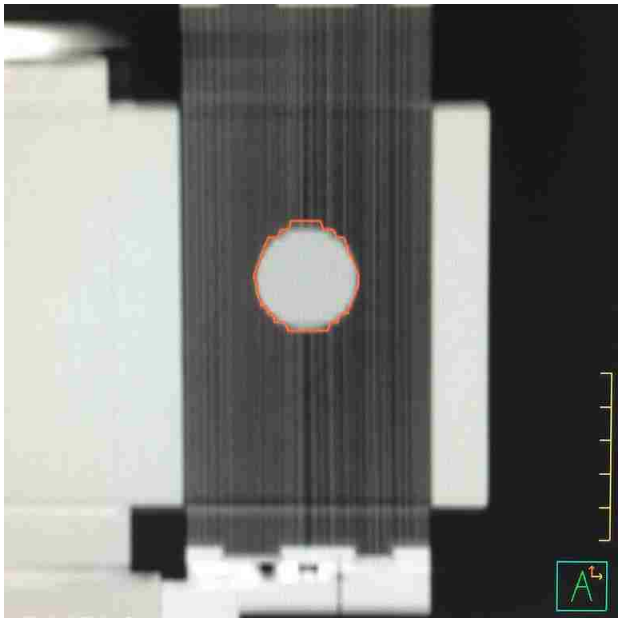

Figure A.5: Exhale phase from 4D CT reference image of the 2 cm Small I/E patient model.

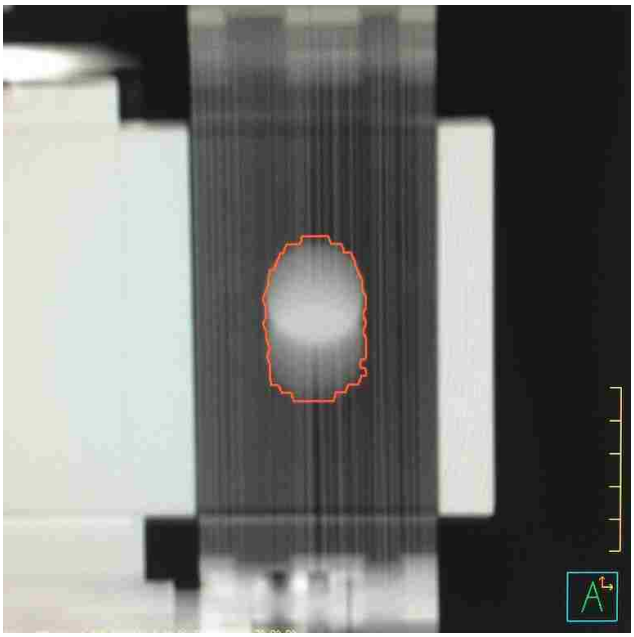

Figure A.6: AIP from 4D CT reference image of the 2 cm Small I/E patient model.

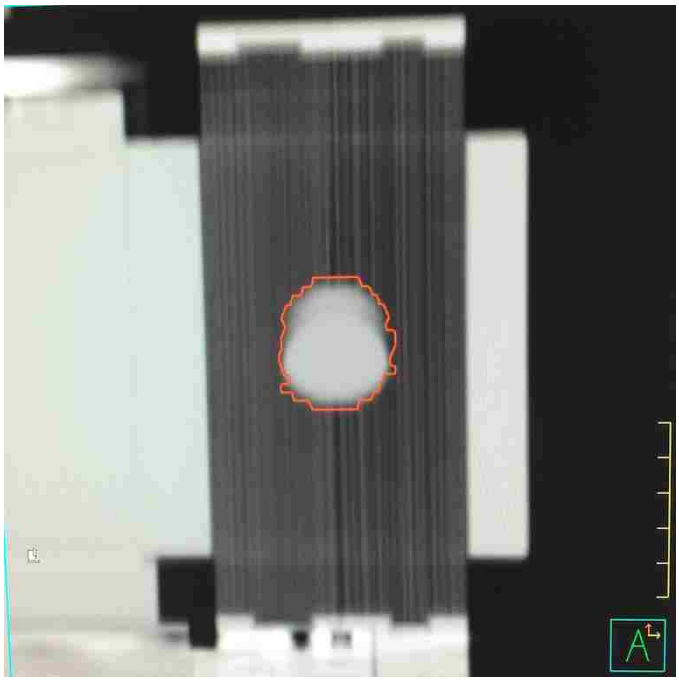

Figure A.7: 3D helical CT reference image of the 1 cm amplitude Medium I/E patient model.

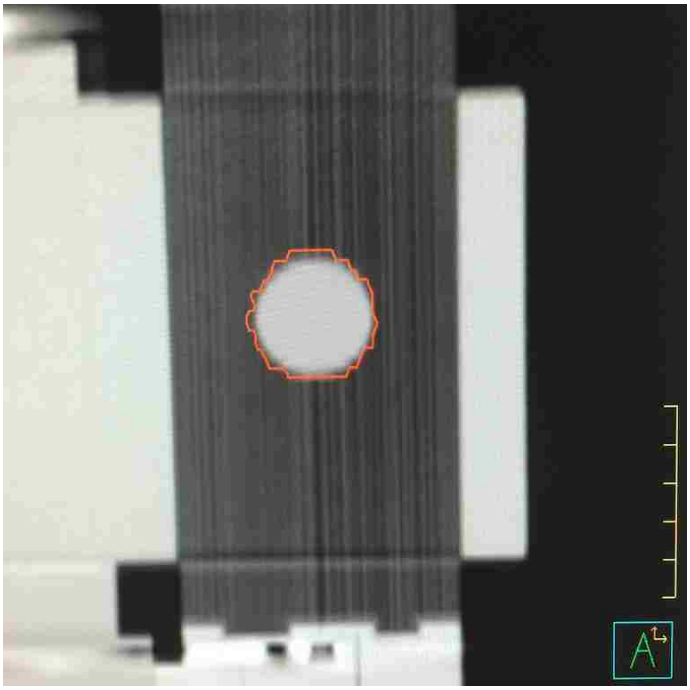

Figure A.8: Exhale from 4D CT reference image of the 1 cm Medium I/E patient model.

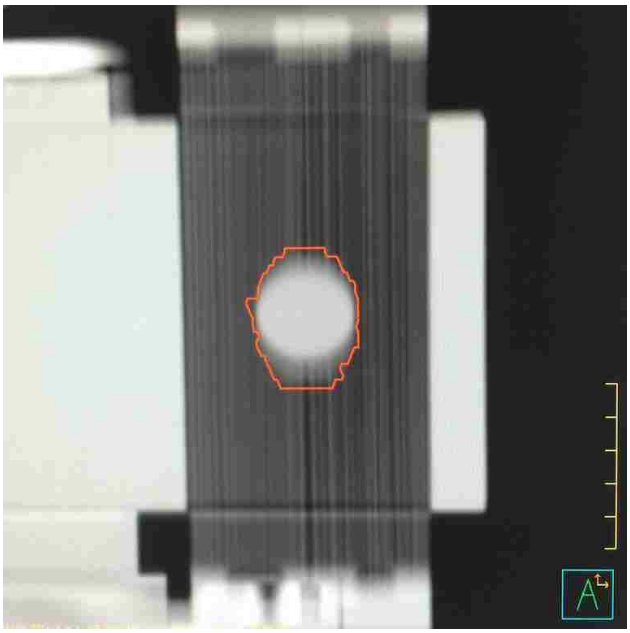

Figure A.9: AIP from 4D CT reference image of the 1 cm Medium I/E patient model.

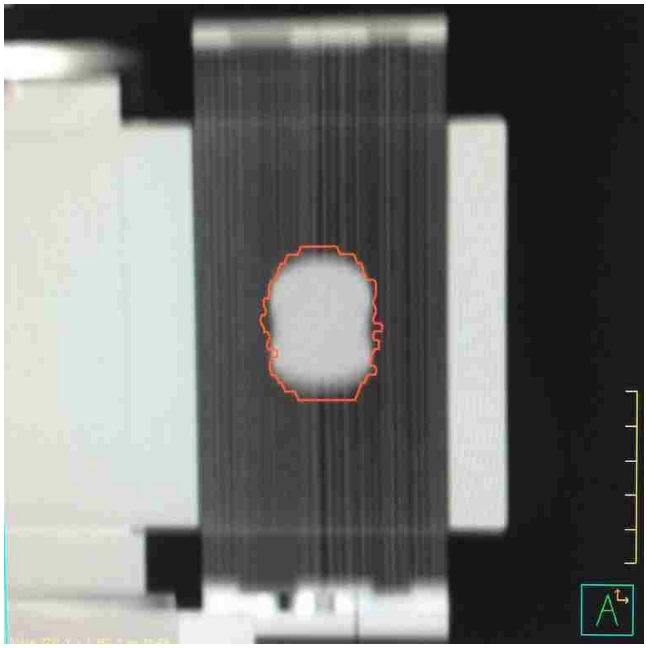

Figure A.10: 3D helical CT reference image of the 2 cm amplitude Medium I/E patient model.

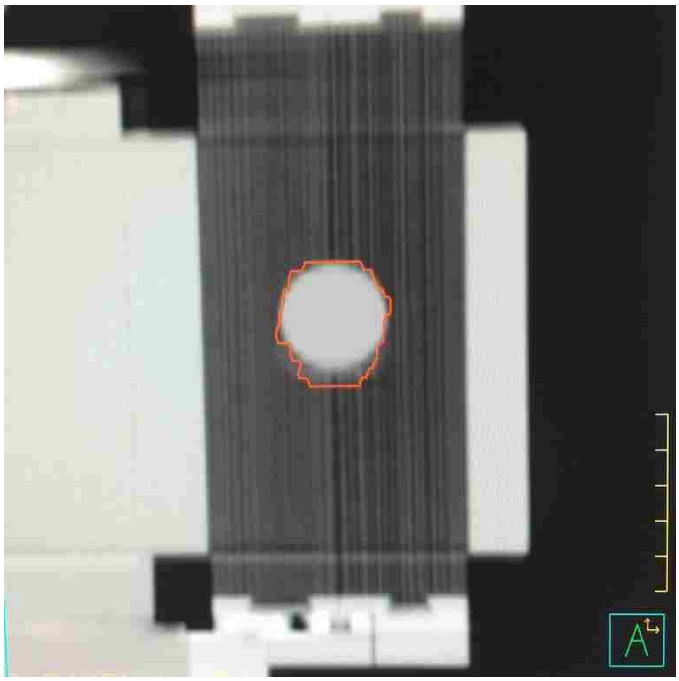

Figure A.11: Exhale from 4D CT reference image of the 2 cm Medium I/E patient model.

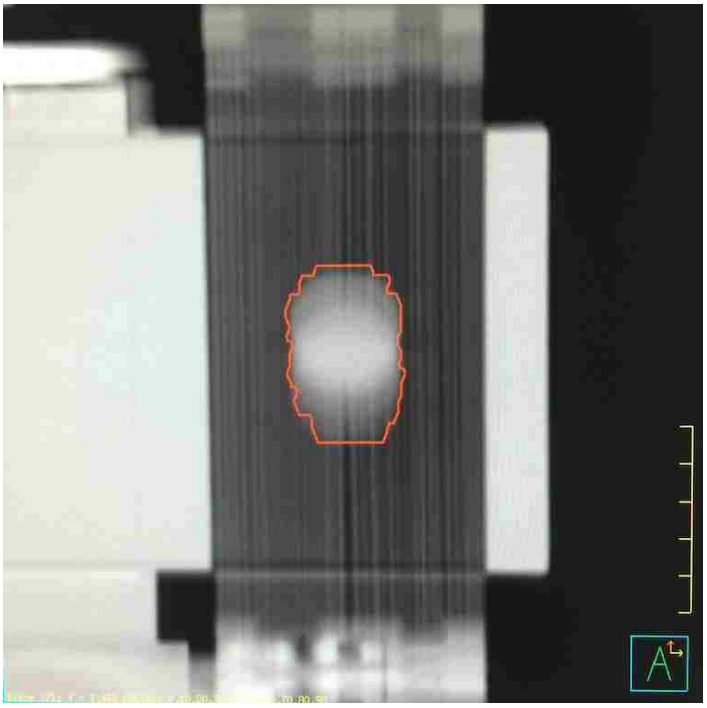

Figure A.12: AIP from 4D CT reference image of the 2 cm Medium I/E patient model.

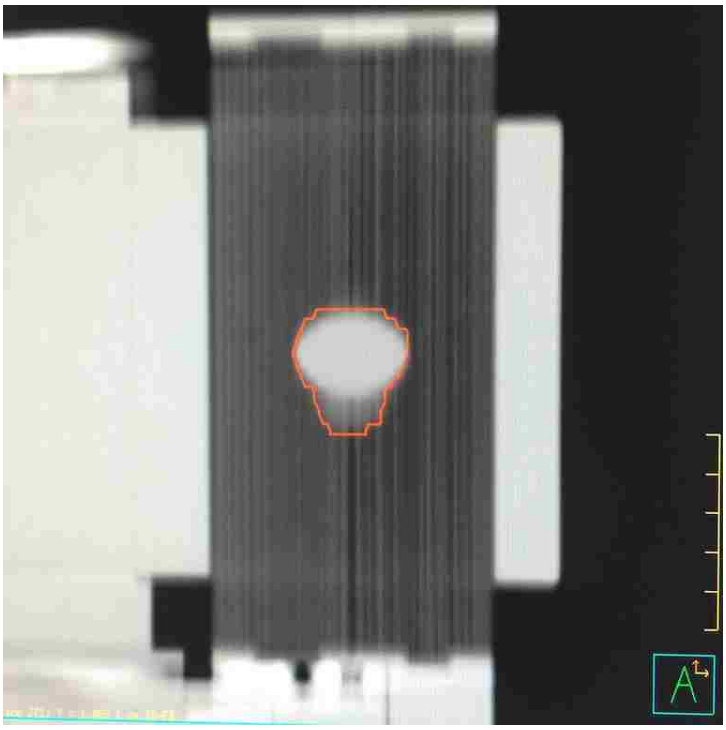

Figure A.13: 3D helical CT reference image of the 1 cm amplitude Large I/E patient model.

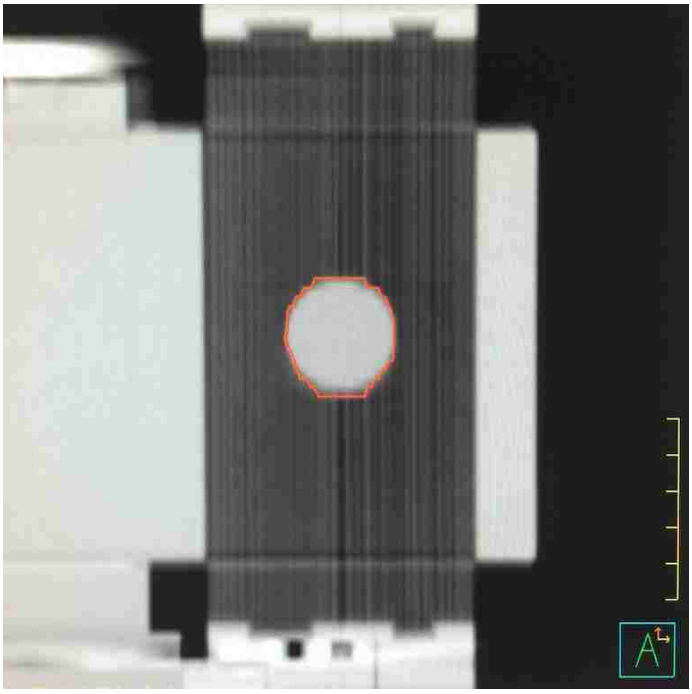

Figure A.14: Exhale from 4D CT reference image of the 1 cm Large I/E patient model.

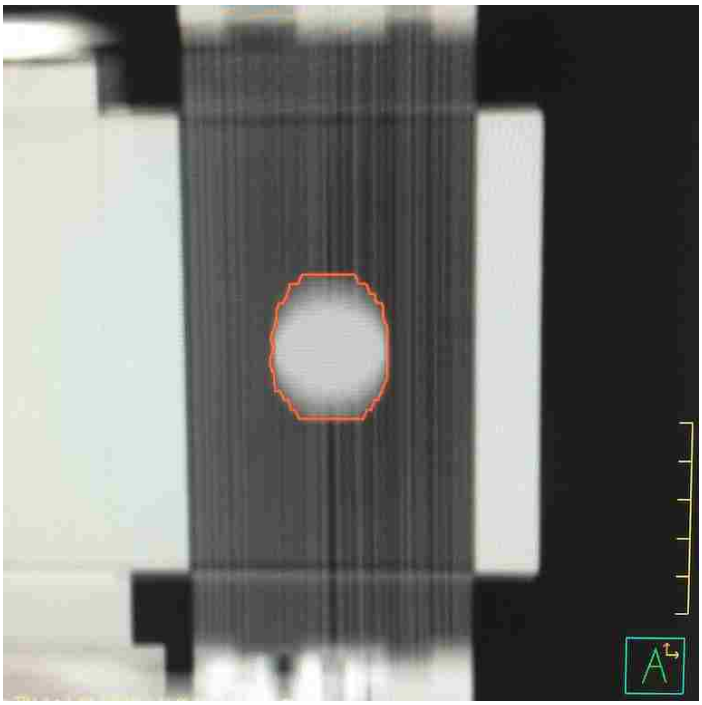

Figure A.15: AIP from 4D CT reference image of the 1 cm Large I/E patient model.

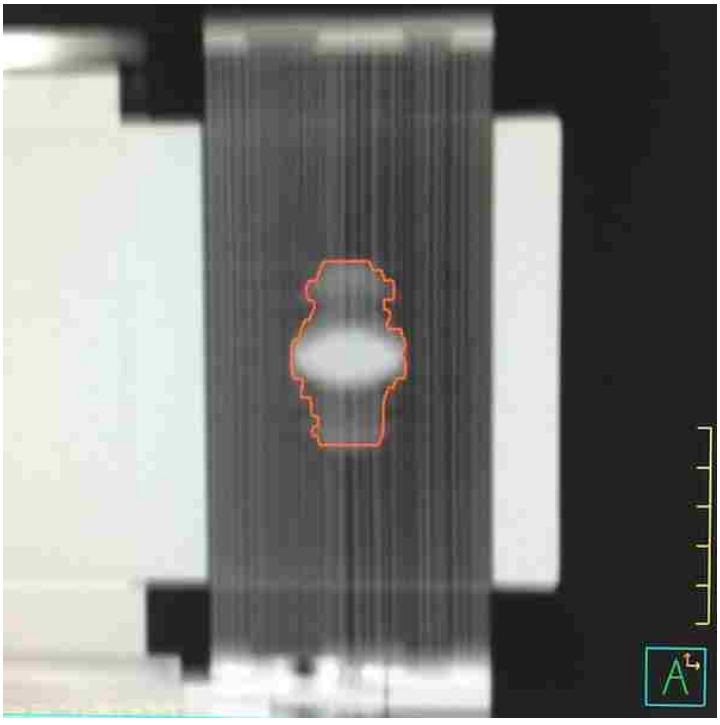

Figure A.16: 3D helical CT reference image of the 2 cm amplitude Large I/E patient model.

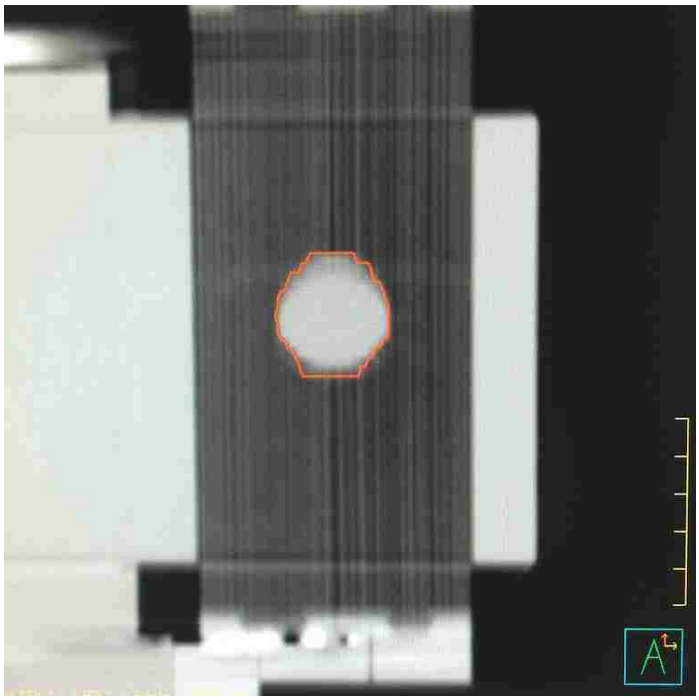

Figure A.17: Exhale from 4D CT reference image of the 2 cm Large I/E patient model.

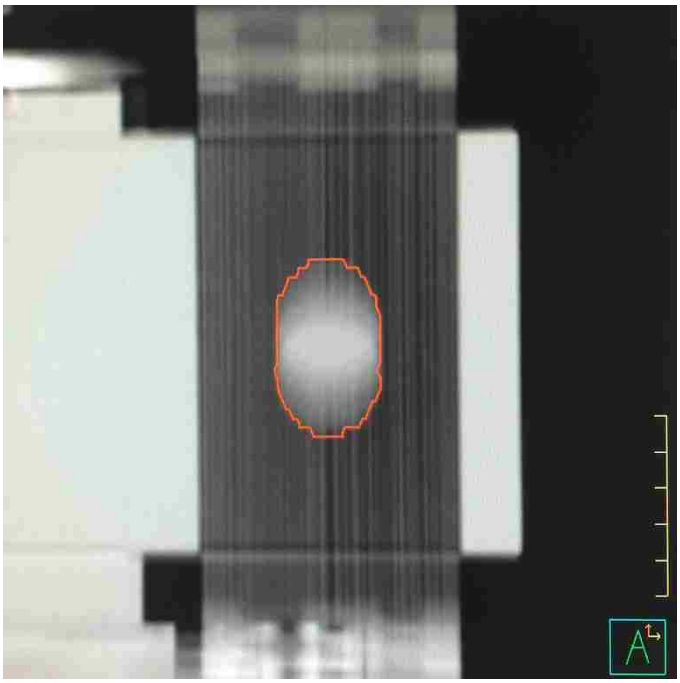

Figure A.18: AIP from 4D CT reference image of the 2 cm Large I/E patient model.

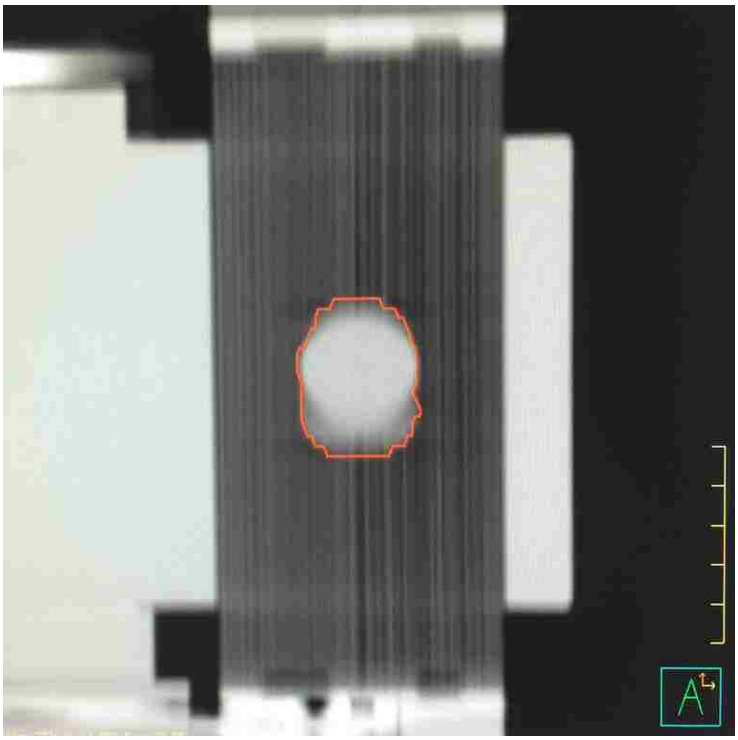

Figure A.19: 3D helical CT reference image for the 2 cm Irregular patient model.

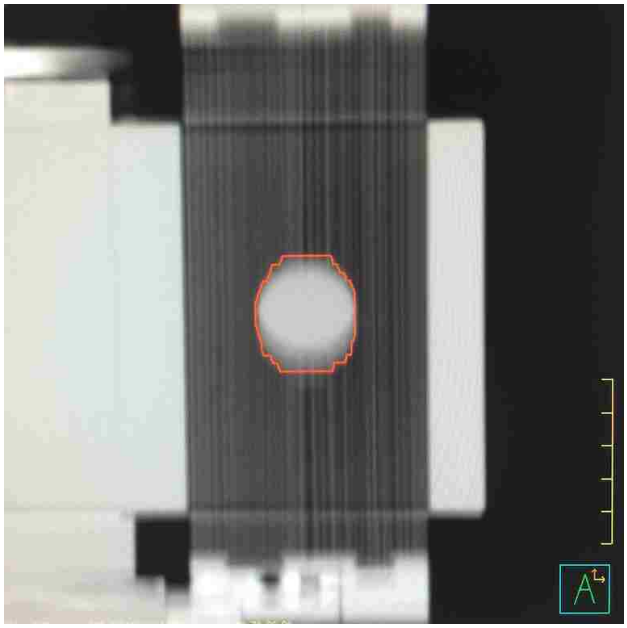

Figure A.20: Exhale from 4D CT reference image for the 2 cm Irregular patient model.

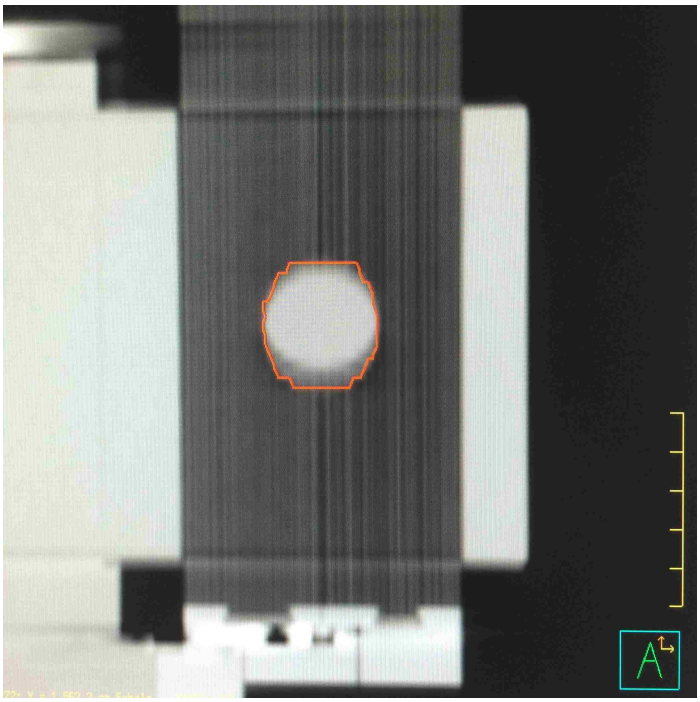

Figure A.21: AIP from 4D CT reference image for the 2 cm Irregular patient model.

APPENDIX B: AIM 2 SUPPLEMENTAL PLOTS

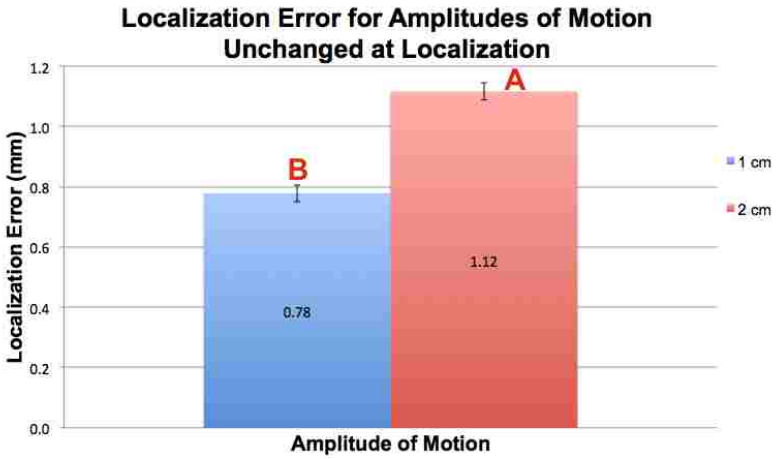

Figure B.1: Localization errors for 1 and 2 cm motion amplitudes unchanged from the reference image. Error bars represent the standard error of the mean. Statistical relationships are displayed above each average (columns that share the same letter are statistically similar).

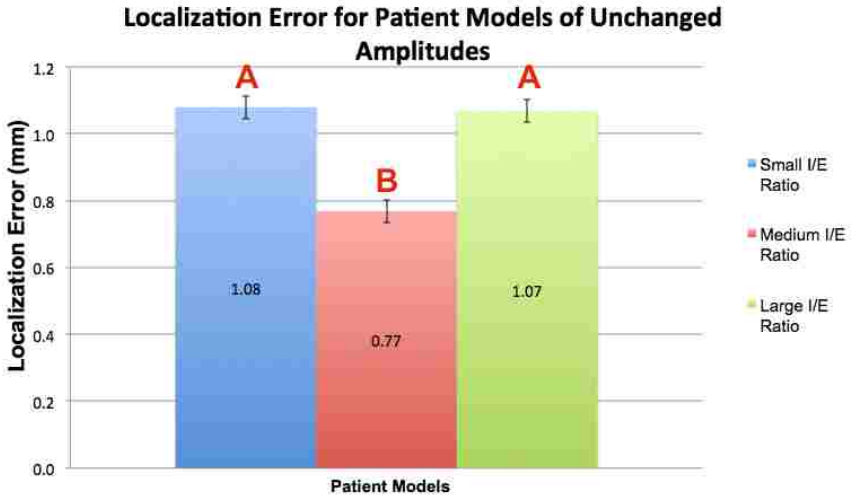

Figure B.2: Localization errors for patient models unchanged from the reference image. Error bars represent the standard error of the mean. Statistical relationships are displayed above each average (columns that share the same letter are statistically similar).

APPENDIX C: AIM 3 SUPPLEMENTAL PLOTS

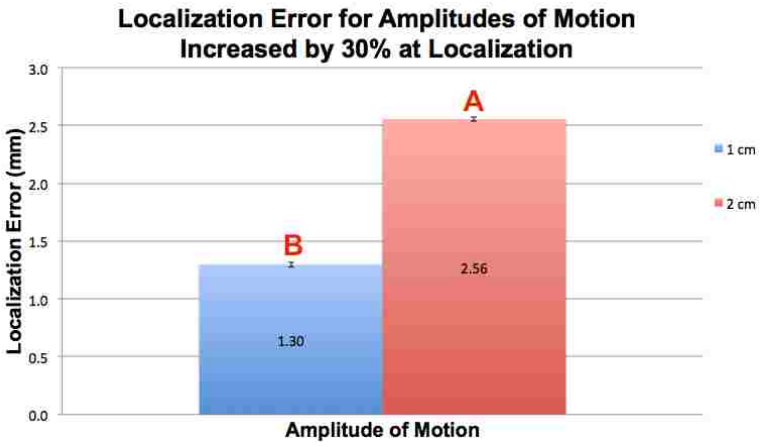

Figure C.1: Localization errors for 1 and 2 cm motion amplitudes increased by 30% from the reference image. Error bars represent the standard error of the mean. Statistical relationships are displayed above each average (columns that share the same letter are statistically similar).

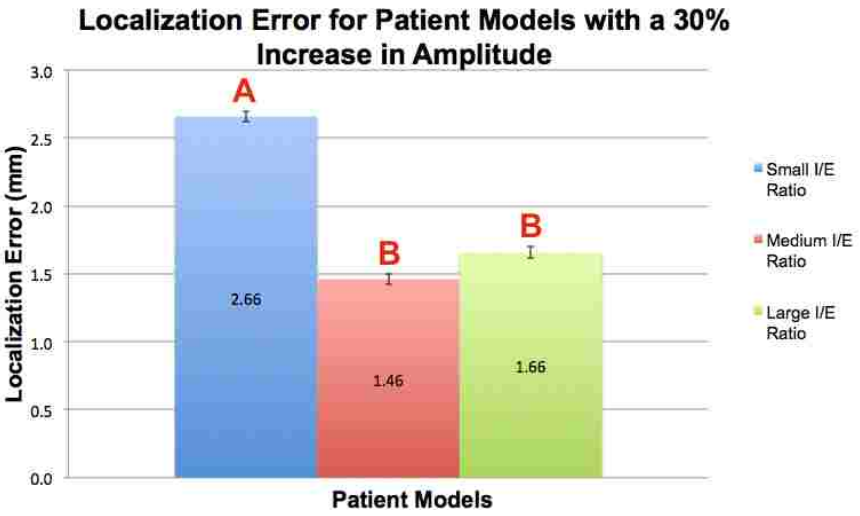

Figure C.2: Localization errors for patient models increased by 30% from the reference image. Error bars represent the standard error of the mean. Statistical relationships are displayed above each average (columns that share the same letter are statistically similar).

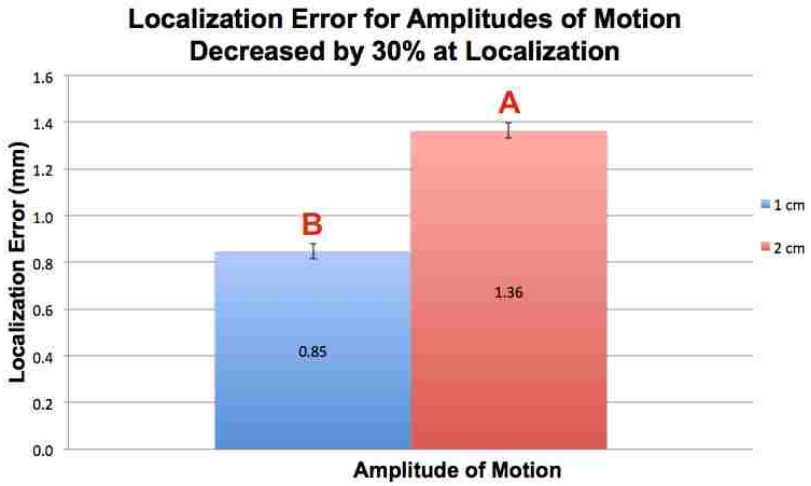

Figure C.3: Localization errors for 1 and 2 cm motion amplitudes decreased by 30% from the reference image. Error bars represent the standard error of the mean. Statistical relationships are displayed above each average (columns that share the same letter are statistically similar).

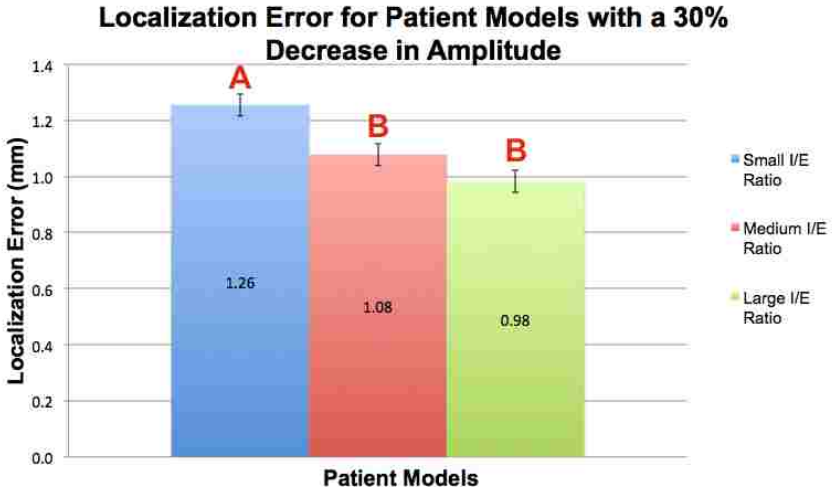

Figure C.4: Localization errors for patient models decreased by 30% from the reference image. Error bars represent the standard error of the mean. Statistical relationships are displayed above each average (columns that share the same letter are statistically similar).

VITA

Runyon Colie Woods is a native of Chapel Hill, North Carolina and received his bachelor's degree in Physics from the University of North Carolina Wilmington in 2012. Upon completion of his undergraduate degree he decided to enter graduate school in the Medical Physics and Health Physics Program in the Department of Physics and Astronomy at Louisiana State University. He is a candidate to receive his master's degree in Medical Physics in August 2015 and will return to North Carolina for his therapeutic medical physics residency at the University of North Carolina at Chapel Hill.